Tectono-thermal evolution of central Transcaucasia: Thermal modelling, seismic interpretation, and low-temperature thermochronology of the eastern Adjara-Trialeti and western Kura sedimentary basins (Georgia)

Published Version:
Gusmeo, T., Schito, A., Corrado, S., Alania, V., Enukidze, O., Zattin, M., et al. (2022). Tectono-thermal evolution of central Transcaucasia: Thermal modelling, seismic interpretation, and low-temperature thermochronology of the eastern Adjara-Trialeti and western Kura sedimentary basins (Georgia). JOURNAL OF ASIAN EARTH SCIENCES, 237, 1-22 [10.1016/j.jseaes.2022.105355].

Availability:
This version is available at: https://hdl.handle.net/11585/896480 since: 2022-10-18

Published:
DOI: http://doi.org/10.1016/j.jseaes.2022.105355

(Article begins on next page)

Tectono-thermal evolution of central Transcaucasia: Thermal modelling, seismic interpretation, and low-temperature thermochronology of the eastern Adjara-Trialeti and western Kura sedimentary basins (Georgia)
(2022) ***Journal of Asian Earth Sciences*****, 237, art. no. 105355**

The final published version is available online at: ***https://dx.doi.org/10.1016/j.jseaes.2022.105355***

Tectono-thermal evolution of central Transcaucasia: Thermal modelling, seismic interpretation, and low-temperature thermochronology of the eastern Adjara-Trialeti and western Kura sedimentary basins (Georgia)

Gusmeo Thomas[a], Schito Andrea[b], Corrado Sveva[c], Alania Victor[d], Enukidze Onise[d], Massimiliano Zattin[e], Pace Paolo[f,g], Cavazza William[a]

[a] Department of Biological, Geological and Environmental Sciences, University of Bologna, Bologna, Italy

[b] Department of Geology and Geophysics, School of Geosciences, University of Aberdeen, Aberdeen AB24 3 UE, UK

[c] Department of Sciences, Geological Sciences Section, Roma Tre University, Rome, Italy

[d] M. Nodia Institute of Geophysics, Ivane Javakhishvili Tbilisi State University, Tbilisi, Georgia

[e] Department of Geosciences, University of Padua, Padua, Italy

[f] Department of Engineering and Geology, "G. d'Annunzio" University of Chieti-Pescara, Chieti, Italy

[g] PACE Geoscience, Chieti, Italy

Abstract:

Structural interference along the boundaries of adjacent tectonic domains generates complex subsidence and exhumation patterns. In this paper we study a key segment of the convergence zone between the interfering south-verging Greater Caucasus and north-verging Lesser Caucasus retro-wedge. The study area comprises the along-strike transition between the Paleogene Adjara-Trialeti back-arc basin and the Oligocene-Neogene Kura foreland basin of eastern Georgia. During the Neogene, despite their difference in age and subsidence mechanisms, both basins have been progressively inverted to various extent within the overall context of the Arabia-Eurasia continental collision. Thermal modelling of borehole data from the Adjara-Trialeti basin allowed to reconstruct two phases of rapid subsidence, late Paleocene-Early Eocene and Middle-Late Eocene, respectively correlated to flexural loading by the Lesser Caucasus retro-wedge and continental rifting. Integration of thermal modelling, apatite fission-track statistical inverse modelling, and seismic interpretation detected a third subsidence phase in the Early Miocene, possibly related to strike-slip tectonics. Thermal maturity data dictate that 1.0-1.3 km of the Adjara-Trialeti sedimentary succession has been eroded since the onset of structural inversion in the mid-Miocene. The burial history of the western Kura Basin outlines intermittent and asymmetrical episodes of flexural subsidence from the Oligocene to the Late Miocene, due to competing loading by the Lesser Caucasus, the Adjara-Trialeti fold-and-thrust belt and the Greater Caucasus. Finally, during latest Miocene times southward propagation of deformation from the Greater Caucasus induced an additional tectonic loading (1.3-1.8 km) due to the emplacement of thin-skinned thrust sheets, mostly eroded during the Plio-Quaternary.

Keywords: *Transcaucasus, Kura Basin, thermal maturity, thermal modelling, fission-track thermochronology, structural interference*

1. Introduction

Tectonic and thermal reconstruction of sedimentary basins evolution during subsidence and structural inversion traditionally refers to clear-cut end-members and ideal models characterised by relatively simple evolutionary patterns, or identify discrete and uniform domains that are then studied more or less independently. Such simplifications can hardly be applied to the boundary zones between adjacent structural domains, where interfering tectonic and subsidence motifs produce complicated temporal-spatial patterns. This is exemplified by the structurally complex Transcaucasian region of central Georgia, an area dominated by the contrasting and partially superposed effects of extension- and compression-driven subsidence, as well as by the structural interference between two oppositely-verging orogenic belts.

The southern Caucasian region is constituted by the Greater and Lesser Caucasus and the intervening Rioni-Kura foreland basins (Fig. 1). This area absorbs a considerable amount (about 15-20%) of the strain associated with the Arabia-Eurasia collision (Reilinger et al., 2006), as testified by GPS vectors indicating an anticlockwise motion relative to stable Eurasia, with northward motion increasing from about 2 mm/yr in the Rioni Basin close to the Black Sea coast to 12 mm/yr in the Kura Basin close to the Caspian Sea coast (Forte et al., 2013; Reilinger et al., 2006). Most deformation in the Caucasian region is accommodated in the domain comprised between the Greater and the Lesser Caucasus (named Transcaucasus; Karakhanyan et al., 2013; Sokhadze et al., 2018).

Transcaucasia (i.e. the region south of the Greater Caucasus) connects the world-class Caspian Basin petroleum province to the east and the underexplored easternmost Black Sea basin to the west, where active hydrocarbon seeps on the seafloor (e.g. Pape et al., 2021) and oil shows in deep-water wells indicate the presence of at least one active petroleum system in the offshore of easternmost Turkey (see Tari et al., 2018, for a review). The oceanographic connection between the Caspian and Black seas closed in the early Late Miocene due to convergence of the facing structural fronts of the south-verging Greater Caucasus and north-verging retro-wedge of the Lesser Caucasus orogenic prism, which incorporated the Adjara-Trialeti FTB (Alania et al., 2021a; Banks et al., 1997; Gusmeo et al., 2021; Nemčok et al., 2013; Tari et al., 2021). Such a convergence is considered a far-field effect of the collision between the Eurasian and Arabian plates along the Bitlis-Zagros suture zone, several hundred kilometres to the south (Alavi, 1994; Cavazza et al., 2018; Dewey et al., 1986; Jolivet & Faccenna, 2000; Okay et al., 2010). This deformation has affected a large swath of the Eurasian hinterland, inducing reactivation of older structures (including structural inversion of pre-existing sedimentary basins) and diffuse strike-slip deformation (Albino et al., 2014; Cavazza et al., 2019).

The aim of this work is to provide quantitative constraints on the burial/exhumation history of the eastern portion of the Georgian Transcaucasus, a tectonically complex area featuring the structural interference between two tectonic domains characterised by different pre-deformation history, deformation timing, exhumation degree, and structural styles. These units are: (i) the E-W-trending Adjara-Trialeti fold-and-thrust belt (FTB), a former rift basin now in the retro-wedge of the Lesser Caucasus, and (ii) the western Kura flexural foreland basin, characterised by distinct subsidence pulses and then deformed by the southward advancing Greater Caucasus frontal structures (Figs. 1 and 2). The geological complexity of the along-strike transition from the Adjara-Trialeti to the Kura inverted basins (Fig. 2) has favoured multiple, often contrasting interpretations regarding the structural layout and the tectonic evolution of the eastern termination of the Adjara-Trialeti FTB, where it plunges eastwards and is covered by south-verging thrusts deforming the Kura Basin (Alania et al., 2021a; Gusmeo et al., 2021; Pupp et al., 2018; Tari et al., 2021).

The study area is ideal to investigate the initial phases of collision between two converging orogenic belts: the south-verging Greater Caucasus pro-wedge and the mostly north-verging Adjara-Trialeti FTB (Alania et al., 2021a; Banks et al., 1997; Gusmeo et al., 2021; Nemčok et al., 2013). Tectonic convergence determined progressive exhumation of the intervening Kura

Basin sedimentary fill. In this context, the retro-wedge of the Lesser Caucasus may also have played an important role (Alania et al., 2021a; Gusmeo et al., 2021).

During the last few decades, a growing academic and industrial interest has provided structural data and burial models on the western Kura basin (Adamia et al., 1992; Boote et al., 2018; Nemčok et al., 2013; Patton, 1993; Pupp et al., 2018; Robinson et al., 1997; Sachsenhofer et al., 2018, 2021). Recent thermochronologic work has determined the structural inversion of the Adjara-Trialeti FTB as mid-Miocene (Gusmeo et al., 2021). Corrado et al. (2021) obtained thermal maturity data on sedimentary successions across the southern Greater Caucasus - Kura - Adjara-Trialeti system. Building on such datasets, in this paper we integrate new multidisciplinary data in the transitional area between the eastern Adjara-Trialeti inverted rift basin and the thin-skinned western Kura Basin in order to provide quantitative constraints on the burial/exhumation history of the eastern Georgian Transcaucasus. The dataset includes (i) low-temperature thermochronologic inverse models, (ii) thermal models of well data, and (iii) a composite geological cross-section of the transition zone built upon the interpretation of three unpublished seismic reflection profiles.

2. Geological background

The study area covers the region where the north-verging Adjara-Trialeti FTB plunges eastward and is covered by the deformed sedimentary rocks of the western Kura Basin (eastern Georgia). In this work we analyse six of the several wells drilled for hydrocarbon exploration (Patton, 1993; Sachsenhofer et al., 2021), three in the Adjara-Trialeti FTB and three in the Kura Basin (Figs. 1 and 2).

The Adjara-Trialeti FTB (Figs. 1 and 2) is a W-E-trending orogenic belt formed as a result of the structural inversion of a former back-arc rift basin developed on the upper (Eurasian) plate of the northern Neotethys subduction zone (Adamia et al., 1981, 2011; Alania et al., 2018; Banks et al., 1997; Barrier et al., 2018; Gusmeo et al., 2021; Lordkipanidze et al., 1989; Nemčok et al., 2013). The pre-rift sedimentary succession features Aptian-Cenomanian volcanic and volcaniclastic rocks, covered by Turonian-to-Early Paleocene limestones and marls (Adamia et al., 1981, 2011; Banks et al., 1997; Yılmaz et al., 2000, 2014). Extension started in the Paleocene, together with the deposition of a thick succession of terrigenous turbidites (the Paleocene-Eocene Borjomi Flysch). The main phase of rifting occurred in the Middle Eocene, characterized by the emplacement of submarine volcanic rocks and shallow mafic-to-intermediate intrusions (Adamia et al., 2011; Banks et al., 1997; Okrostsvaridze et al., 2018; Yılmaz et al., 2000, 2014). In the Late Eocene, mostly epiclastic turbidites with minor marls were deposited in the eastern sector of the Adjara-Trialeti basin. In Oligocene-Early Miocene times shales, siltstones and fine-grained sandstones were deposited in a mainly anoxic/disoxic environment (Pupp et al., 2018; Sachsenhofer et al., 2018, 2021), interbedded with fine-grained terrigenous turbidites. The post-rift phase lasted from the Oligocene to the Early Miocene and was followed by structural inversion since Middle Miocene times (Gusmeo et al., 2021). Despite having an independent origin, the Adjara-Trialeti FTB was then incorporated in the retro-wedge of the Lesser Caucasus (Alania et al., 2021a).

The domain comprised between the Greater Caucasus and the Lesser Caucasus (Transcaucasia) is constituted by an intermontane depression extending from the Black Sea to the Caspian Sea (Fig. 1). The depression is divided by the Dzirula Massif, a polymetamorphic basement salient which separates the Kura and Rioni flexural foreland basins (Adamia et al., 2010, 2011; Alania et al., 2017; Banks et al., 1997; Nemčok et al., 2013; Rolland et al., 2011). The two basins - mostly filled by Oligocene-to-Recent sediments - plunge to the east and west, respectively, and developed as a flexural response to both the Greater Caucasus to the north and the Lesser Caucasus to the south (Adamia et al., 2010; Banks et al., 1997; Nemčok et al., 2013).

In the Kura Basin (Figs. 1 and 2) Oligocene-Lower Miocene clastic (shales, siltstones and fine-grained sandstones) and evaporitic rocks were deposited in the anoxic-dysoxic environment of the Paratethys, and are locally known as the Maikop series (Pupp et al., 2018; Sachsenhofer et al., 2018). Their thickness can reach up to 2.5-3.5 km in the Georgian sector of the Kura Basin (Adamia et al., 2010).

During Middle to early Late Miocene times (Chokrakian-Sarmatian) further 1.5-2.2 km of shales and fine-grained siliciclastics (sandstones), intercalated in the uppermost sections with mainly calcareous units (mudstones, marls and oolitic limestones and locally with coarse-grained rocks), were deposited within the Kura Basin (Adamia et al., 2010; Alania et al., 2017). Since the Late Sarmatian (Tortonian) ongoing convergence between the Greater and Lesser Caucasus forced the final uplift of the Dzirula Massif and the Kura Basin started plunging towards the Caspian Sea, as demonstrated by the progressive marine regression within the basin from west to east (Adamia et al., 2010; Alania et al., 2017; Barrier et al., 2018; Nemčok et al., 2013; Shatilova et al., 2020). At the same time, within the Kura Basin began the widespread deposition of coarse-grained clastic deposits, eroded from the adjacent orogenic belts.

Continental conditions prevailed from the Late Sarmatian to the present, interrupted only in the Akchagylian-Apsheronian (Late Pliocene-Early Pleistocene) by a short-lived shallow marine transgression, probably in response to the rapid growth and advancement of the Greater Caucasus and the ensuing subsidence in the foreland area (Adamia et al., 2010; Avdeev and Niemi, 2011; Nemčok et al., 2013; Sukhishvili et al., 2020; Trikhunkov et al., 2021).

Continuous convergence between the Greater and Lesser Caucasus caused incremental deformation of the Kura foreland basin. Thick-skinned deformation occurred in the Sarmatian followed by thin-skinned deformation from the Late Sarmatian-Meotian (Nemčok et al., 2013). In the final stages of convergence, the Greater Caucasus deformation propagated into the northern Kura Basin forming the Kura south-vergent thin-skinned foreland FTB (Kakheti ridge, Fig. 2), developed since the Middle Miocene, with peak deformation in the Late Miocene-Pliocene (Alania et al., 2017). A Late Pliocene-Pleistocene acceleration of uplift has also been pointed out in this belt (Sukhishvili et al., 2020), probably linked with coeval enhanced uplift in the Greater Caucasus and subsequent propagation of deformation. The Kakheti ridge and the Adjara-Trialeti structures interfere in the Tbilisi area, creating an outstanding example of incipient collision between two facing orogenic belts (Alania et al., 2021a) (Figs. 1 and 2).

The study area is tectonically active. GPS vectors in the eastern Adjara-Trialeti FTB are N/NNE-oriented and indicate velocities in the order of 4-6 mm/yr, decreasing to the north in the Kura Basin to 2-4 mm/yr (Reilinger et al., 2006; Sokhadze et al., 2018). Historical earthquakes in the study area are of moderate intensity, with the last major event recorded in 2002 in the surroundings of Tbilisi (Fig. 2) yielding a magnitude of 4.5 (Tibaldi et al., 2019). Present-day heat flow is ca. 50 mW/m^2 in the eastern Adjara-Trialeti FTB and ca. 40-45 mW/m^2 in the western Kura Basin (Melikadze et al., 2015; Sangin et al., 2018; Yükler et al., 2000), and crustal thickness ranges between ~ 45 and 50 km in the area of study (Adamia et al., 2017; Motavalli-Anbaran et al., 2016).

2.1 Wells stratigraphy

The six wells analysed in this study are, from south to north, Kumisi 1, Kumisi 2 and Patardzeuli-E1 in the eastern Adjara-Trialeti FTB, and Satskhenisi 102, Satskhenisi 101 and Norio 200 in the western Kura Basin (Figs. 2 and 3).

Wells drilled in the eastern Adjara-Trialeti FTB are generally deeper (ca. 1.8 to 5 km) than the ones in western Kura Basin (ca. 1 km) and the thickest sedimentary succession (5020 m) was drilled in the Patardzeuli-E1 well (Korelskiy et al., 2019).

In the Adjara-Trialeti FTB, the oldest rocks were drilled in the Kumisi 1 well and are Late Cretaceous volcanics and volcaniclastics followed by limestones and marls (Fig. 3). The Paleocene section has similar thickness (ca. 250 m) in both Patardzeuli-E1 and Kumisi 1 wells, but in Patardzeuli-E1 it is entirely made of limestones, whereas in Kumisi 1 it is composed of marls at the base, followed by shales and siltstones. The Early Eocene section is thicker in Patardzeuli-E1 (ca. 1800 m) than in Kumisi 1 (ca. 730 m). In Patardzeuli-E1 the lower portion of the Early Eocene section is mostly characterised by limestones and marls, passing to mostly fine-grained siliciclastic rocks in the upper part; in Kumisi 1 it is made of alternating sandstones and shales (flysch facies). The Middle Eocene is found in all three wells drilled in the eastern Adjara-Trialeti FTB, and it is thicker in Patardzeuli-E1 (ca. 700 m) than in Kumisi 1 and 2 (ca. 250 m). It is mainly composed of tuffs and other volcaniclastic rocks, sporadically interbedded with sandstones and shales (Fig. 3). The thickness (700-900 m) and composition of the Late Eocene section are similar in all three wells. The lower portion (ca. 230 m) in Kumisi 1 is entirely made of shales and siltstones, whereas the upper part (Tbilisi Suite) is composed of alternating shales, sandstones, and siltstones with marls interlayers. In Patardzeuli-E1 and Kumisi 2 the Late Eocene is lithologically similar to the Tbilisi Suite of Kumisi 1 (Fig. 3).

The Maikop Series is the only succession found in all six wells and it is composed of shales, siltstones, and fine-grained sandstones. The thickness of the succession ranges from ca. 550 m (Kumisi 1) to >1200 m (Satskhenisi 102). The Maikop Series is probably incomplete in all wells except for Norio 200. In the Satskhenisi 101 and 102 wells the lower part of the succession (representing the Lower Maikop, hence the Lower Oligocene section) is missing, whereas in Kumisi 1, Kumisi 2 and Patardzeuli-E1 at least part of the uppermost section was eroded away, as demonstrated by unconformable surfaces.

Middle Miocene rocks (Chokrakian, Karaganian and Konkian) are found almost exclusively in the Norio 200 well, where they are entirely made of shales and siltstones. The same well is topped by Sarmatian (late Middle-early Late Miocene) shales and siltstones, with frequent alternations of sandstones and conglomerates in the uppermost portion. Chokrakian shales are found also in the Satskhenisi 101well (Fig. 3).

Finally, Akchagylian-Quaternary conglomerates are present in the Patardzeuli-E1 well, whereas very thin Quaternary deposits constitute the top of the Kumisi 1 well (Fig. 3).

3. Materials and methods

3.1 Apatite fission-track analysis and modelling

Fission tracks are linear radiation damages within the crystal lattice, caused by the nuclear fission of radioactive isotope ^{238}U, which can be etched and counted with an optical microscope (Donelick et al., 2005). Neutron irradiation is used to induce the decay of ^{235}U, generating radiation damages on the surface of an external detector. Grain-by-grain determination of both spontaneous and induced fission-track densities yields a single-grain age representing the cooling of the grain below a closure temperature of ~100°C. Apatite grains are concentrated through crushing and sieving, followed by hydrodynamic, magnetic, and heavy-liquids separation. Then apatites are embedded in epoxy resin, polished, and etched in 5N HNO_3 at

20°C for 20s. The external detector method was applied: following irradiation at the Radiation Center of Oregon State University (Donelick et al., 2005) and etching of the mica detector in 40% HF at 20°C for 45 min, spontaneous and induced fission tracks were counted under a Zeiss Axioscope optical microscope at x1250 magnification. Central ages (Fig. 2, Table 1) were obtained using the Radial Plotter software (Vermeesch, 2009).

Fission tracks in apatites have the same initial length of about 16 µm (Donelick et al., 1999; Ketcham et al., 1999) but at about 60°C they start to anneal at a rate that is proportional to temperature. Over geological time periods, partial annealing of fission tracks occurs at temperatures between about 60 and 120°C (the Partial Annealing Zone or PAZ; Gleadow & Duddy, 1981). Since track shortening is a function of the intensity and duration of heating, the measurement of fission-track lengths and the numerical modelling of their frequency distribution give quantitative information on the thermal evolution in the PAZ temperature range. Modelling procedures find a range of cooling paths compatible with the fission-track length frequency distribution (Ketcham, 2005).

In this work, we provide additional constraints on the thermal history of two samples (TU504 and TU505) already included in the dataset of Gusmeo et al. (2021). These two samples were selected because of their peculiar positions within the study area. Since only their central ages were available, further mounts of apatite grains for each sample were produced, etched and analysed under a Zeiss Axioscope optical microscope in order to measure enough horizontally confined tracks for statistical inverse modelling. Inverse modelling of track length data was performed using the HeFTy program (Ketcham, 2005), which generates a number of possible T-t paths by running a Monte Carlo algorithm using fission-track lengths and ages as input data. Predicted AFT data were calculated according to the Ketcham et al. (2007) annealing model for fission tracks revealed by etching. Dpar values (i.e. the etch pit length) were used to define the annealing kinetics. Broad T-t boxes were used for the pre- and postdepositional history of the analysed samples in order to limit any user-dependent forcing on the program. Details on parameters and constraints used for both models, compiled following the protocol of Flowers et al. (2015), can be found in the Supplementary Materials (Tables ST6 and ST7).

3.2 Thermal Modelling

3.2.1 Calibration data from Rock-Eval Pyrolysis and optical analyses

Thermal model calibration is generally based on the assumption that thermal maturity at different depths of a stratigraphic section allows to fit a maturity curve, giving an insight on the maximum thermal exposure and heating regimes experienced by the sediments during burial. For this purpose, vitrinite reflectance ($VR_o\%$) data are generally used, given their high sensitivity to thermal perturbations. However, when such data are absent they can be replaced by other thermal maturity indicators (e.g. Tmax, biomarkers, illite % in illite-smectite mixed layers, Raman and FTIR parameters) properly converted into $VR_o\%$ (see Corrado et al., 2020; Schito et al., 2016).

Calibration data for thermal models were provided by the Georgian Oil & Gas Company. They were obtained from five wells drilled for hydrocarbon exploration in the western portion of the Kura Basin and in the eastern Adjara-Trialeti FTB (Fig. 2, Table 2). From south to north the wells are: Kumisi 1, Kumisi 2, Patardzeuli-E1, Satskhenisi 102, Norio 200. Calibration data were acquired in different laboratories and are described in industrial reports and published papers: Stratochem Egypt (2014) for Kumisi 1 well; Sachsenhofer et al. (2021) for Kumisi 2, Patardzeuli-E1 and Norio 200 wells; DIG (2014) for Satskhenisi 102 well. Part of the dataset (relative only to the Maikop sections) was also reported by Corrado et al. (2021).

Most of the thermal maturity data derive from Rock-Eval Pyrolysis, except for the Satskhenisi 102 well where additional vitrinite reflectance measurements are available (Table 2). In detail, more than two hundred Rock-Eval Pyrolysis data and ten vitrinite reflectance measurements are available, acquired from cuttings representative of the Eocene-Early Miocene interval (Table 2, Suppl. Mat. Tables ST1, ST2, ST3, ST4, ST5). The Satskhenisi 101 well was not modelled as no thermal maturity data were available.

Rock-Eval Pyrolysis is the most used quantitative method for kerogen characterization. It is based on the relative intensity and distribution of three peaks (S1, S2 and S3), artificially generated at different lab temperatures from a whole rock specimen containing kerogen. The S2 peak relates to the hydrocarbon residual potential of a source rock, whereas S1 records the amount of already generated hydrocarbons. Tmax is calculated from the temperature corresponding to the maximum of the S2 envelope (e.g. Behar et al., 2001) and can be used as a thermal maturity indicator, at least when Total Organic Carbon (TOC) is higher than 0.5% (Hunt, 1996). The TOC refers to the weight percentage (wt %) of the organic carbon present in the rock (e.g. Langford and Blanc-Velleron, 1990). The Hydrogen Index (HI) is defined as the ratio between the area of the S2 peak and the TOC. The most used diagram for kerogen classification is the modified Van Krevelen's one, which is based on the Hydrogen Index (HI) and the Oxygen Index (OI) (Abdullah et al., 2017; Tissot and Welte, 1978).

Pseudo-Van Krevelen diagrams (OI vs HI, Tmax vs HI, and TOC vs S2) were used to assess the type of kerogen for each data (Fig. 4; Suppl. Mat. Figs. S1, S2, S3, S4, S5).

Vitrinite reflectance (VR_o%) measures the reflectivity under incident light of huminite-vitrinite group macerals that derive from upper plants (Type III kerogen). VR_o% is known to be well correlated with the stages of hydrocarbon generation and is by far the most known and used thermal maturity indicator (Bertrand et al., 2010; Borrego and Cook, 2017; Corrado et al., 2020; Dow, 1977).

3.2.2 Modelling procedures

Five wells have been modelled matching Tmax and VR_o% data with calculated maturity curves at different depths using the Basin Mod 2-D software package. For models' calibration Tmax data were first converted into VR_o% values. No single equation exists for such conversion, since it depends on kerogen type. According to the most recent review (Yang and Horsfield, 2020) and considering a prevalent type III (or II/III) kerogen (Fig. 4), the onset of the oil window (VR_o% = 0.55) can be set at a Tmax value of 430 °C, whereas the immature stage at a Tmax value of 420 °C roughly coincides with a VR_o% value of 0.4 and the onset of the wet gas stage (VR_o% = 1.3) is set at a Tmax value of 460 °C. These values are then correlated by a least squared curve.

Tmax data can have a large spread, as outlined in the dataset presented in this study. The causes of such spread are multiple and cannot be resolved with the available data. In general, data indicating higher maturity (with respect to the mean maturity trend) can be ascribed to the presence of reworked organic matter, whereas relatively low values can be due to carryover effects (i.e. presence of heavy hydrocarbons) or to high H or S content (Yang and Horsfield, 2020). Given the higher uncertainties (with respect to VR_o%) derived from the use of Tmax data for thermal models calibration, different scenarios have been tested and framed according to the geological evolution of the two studied areas: the eastern Adjara-Trialeti FTB and the western Kura Basin (Figs. 5 and 6; see below and Discussion).

Mixed lithologies were reproduced from the relative abundance of sandstones, limestones and shales as shown in Table 3 and rock decompaction follows Sclater and Christie (1980). Seawater depth variations were not taken into account given that the long-term thermal evolution of a sedimentary basin is mainly affected by sediment thickness rather than by water depth (Butler, 1991). A surface temperature of 12°C and a sediment-water interface temperature of 5°C were adopted, and vitrinite reflectance maturation through time was modelled according to the Easy %Ro method (Burnham and Sweeney, 1989; Sweeney and Burnham, 1990).

Present-day heat flow (HF) for the eastern Adjara-Trialeti FTB is ~ 50 mW/m^2 (Melikadze et al., 2010; Sangin et al., 2018; Yükler et al., 2000), and between 40 and 45 mW/m^2 for the studied sector of the western Kura Basin (Kutas, 2010). Since direct constraints on the HF evolution through time in the two geologic domains analysed are not available, two scenarios were assumed and tested in the two domains to allow a systematic comparison. In the first scenario, the HF was set at the present day value of 50 mW/m^2 in the Adjara-Trialeti FTB and 45 mW/m^2 in the Kura Basin (Kutas, 2010; Melikadze et al., 2015; Sangin et al., 2018; Yükler et al., 2000) and kept constant through time. In the second scenario, a HF peak of around 70 mW/m^2 was assumed at about 45 Ma (i.e. during the main phase of Adjara-Trialeti rifting, see Section 2), followed by a gradual decrease in HF up to the present-day value according to the McKenzie model (McKenzie, 1978).

In all the studied wells an additional overburden was required in order to fit thermal maturity data. A sensitivity analysis was then performed, showing (for each HF scenario and each well) different maturity curves assuming different amounts of additional burial (Figs. 5 and 6). See Section 4.2.2 for further discussion on this topic and the results of the sensitivity analyses.

3.3 Seismic interpretation

Three broadly N-S trending depth-migrated seismic reflection profiles (from north to south, lines 3004, 13 and 1401; Figs. 2 and 7) were obtained from the Georgian Oil & Gas Company. Lines 3004 and 13 cross the frontal part of the eastern Adjara-Trialeti FTB and the southernmost Kura Basin, passing through the location of the Norio 200 well; Line 1401 crosses the south-eastern Adjara-Trialeti FTB, passing through the location of the Kumisi 1 well and close to the Kumisi 2 well (Fig. 2).

Seismic interpretation is constrained by surface geology (e.g. Alania et al., 2021a; Banks et al., 1997; Nemčok et al., 2013; USSR Geological Survey, 1971), exploration wells and the application of fault-related folding models (Butler et al., 2018; Shaw et al., 2006). Line 1401 was interpreted alone, whereas lines 13 and 3004 were combined and interpreted together (Fig. 7). Linking together the three interpreted seismic profiles a geological cross-section was then built, showing the structural relationships between the eastern Adjara-Trialeti FTB and western Kura Basin tectonic domains (Fig. 7).

4. Results

4.1 Apatite fission-track analysis and modelling

Analytical results of apatite fission-track analysis are reported in Table 1. The χ^2 statistical test (Galbraith, 1981) indicates that a single population of grains is present in the analysed samples. AFT central ages provide meaningful information from a geological viewpoint if the sample experienced fast cooling through the PAZ but can be misleading if the sample resided within the PAZ for a long time or experienced moderate reheating at temperatures lower than 120°C (Gleadow et al., 1986). To avoid such potential issues, more complete thermochronological constraints were obtained through statistical modelling of fission-track length distributions.

Sample TU504 is a sandstone collected north of the town of Rustavi in the eastern Adjara-Trialeti FTB (Fig. 2). Its depositional age, in the local Paratethyan stratigraphy, is Sakaraulian (USSR Geological Survey, 1971), which corresponds to the base of the Burdigalian (Adamia et al., 2010): hence an age of 20-18 Ma was assigned to this sample. Sample TU504 yielded an AFT central age of 36.3 ± 2.8 Ma (Fig. 2, Table 1), older than its stratigraphic age, which indicates that it was not buried enough to completely reset the AFT system. The very high $P(\chi^2)$ value of 99.98% (Table 1) and the absence of dispersion (0%) (Fig. 8) indicates the presence of only one population of grains. Partially to non-reset detrital samples containing a single population of grains may suggest that they were fed by one thermally coherent sediment source-area. The mean confined tracks length, on a total number of 83 horizontally confined tracks, is 13.34 ± 0.17 µm (Table 1) and the track-length frequency distribution is bimodal, with two peaks centred at ~12 and 15 µm (Fig. 8). Inverse modelling, integrating fission-track data and stratigraphic age (Fig. 8, Table ST6), shows a phase of heating due to sedimentary burial after deposition (20-15 Ma), followed by rapid cooling since 15 Ma. Although with the available data we cannot be certain that the apatite grains derived from a thermally coherent source, since a number of assumptions have to be verified (see a comprehensive review in Malusà and Fitzgerald, 2020), the very high $P(\chi^2)$ value, the absence of dispersion and other independent geologic evidence (see Sections 2 and 5.2) allow us to be reasonably confident regarding the inverse modelling results which suggest an Early Eocene cooling (best-fit curve; Fig. 8) in the original sediment source area.

Sample TU505 is a middle-late Oligocene (30-23 Ma) (USSR Geological Survey, 1971) sandstone (Fig. 2), collected ~15 km north of sample TU504, yielding an apatite fission-track central age of 39.6 ± 3.6 Ma (Fig. 2, Table 1) which is older that its stratigraphic age, indicating that burial was not enough to completely reset the AFT system. The very high $P(\chi^2)$ value of 97.99% (Table 1) and the absence of dispersion (0%) (Fig. 9) confirm that this sample contains only one population of grains, thus suggesting a thermally coherent source. The mean confined tracks length, based on 67 horizontally confined tracks, is 13.41 ± 0.18 µm (Table 1) and the track-length frequency distribution is bimodal, with two peaks centred at ~12 and 15 µm (Fig. 9). TU505 modelling results are broadly in agreement with the ones of sample TU504. Inverse modelling, integrating fission-track data and stratigraphic age, (Fig. 9, Table ST7) shows fast burial/heating from about 28-25 to 20-19 Ma, followed by relatively rapid cooling since 20-19 Ma. Under the same assumptions explained for sample TU505 (Malusà and Fitzgerald, 2020), the very high $P(\chi^2)$ value and other independent geologic evidence (see Section 5.2) allow us to be reasonably confident about the best-fit t-T path in the statistical inverse modelling results suggesting late Paleocene-Early Eocene rapid cooling in the original source of detritus (Fig. 9).

4.2 Thermal modelling

4.2.1 Calibration data

Maturity data used for modelling calibration consist of Tmax and VR_o% (only for Satskhenisi 102 well) data which were provided by the Georgian Oil & Gas Company. Only Tmax data from samples with TOC >0.5% were used as input data for modelling calibration.

Analytical details of calibration data are summarised in Table 2, where the minimum, maximum and average values of each parameter are reported, whereas the complete list of single analytical data is enclosed in the Supplementary Materials (Tables ST1, ST2, ST3, ST4 and ST5). Further details are reported in Corrado et al. (2021), DIG (2014), Sachsenhofer et al. (2021) and Stratochem Egypt (2014).

4.2.2 Thermal models calibration

In this study, Tmax data delineate a maturity trend in three out of five wells (i.e. Kumisi 1, Patardzeuli-E1 and Satskhenisi 102), whereas in Kumisi 2 and Norio 200 wells they only provide information on the thermal maturity along restricted stratigraphic sections (Late Eocene and Early Oligocene, respectively; Figs. 5 and 6; Table 2).

In the three wells (Kumisi 1, Kumisi 2 and Patardzeuli-E1) from the eastern Adjara-Trialeti FTB, two main constraints derive from Tmax data: the top of the Maikop section shows values generally lower than the onset of the oil window (i.e. below 430 °C), whereas the bottom of the Late Eocene section is close to the peak of oil generation (around 440 °C). The Late Eocene section yields a higher degree of uncertainty, due to the high data spread in Patardzeuli-E1 well and to the few data available in the Kumisi 1 well, although a better constrain on the maturity level is given for this section by the clear cluster at the bottom of the Late Eocene section in the Kumisi 2 well. To fit such maturity trends, depending on the assumed HF scenario (see Section 3.2.2), different amounts of additional burial are required (Fig. 5). In the constant HF scenario, maturity data are best fitted with 2000m of additional burial in the Kumisi 1 well and 1500m of additional burial in the Kumisi 2 and Patardzeuli-E1 wells (Fig. 5a, c, e). On the other hand, in the rifting HF model (the scenario with a HF peak around 45 Ma) the additional burial required to fit thermal maturity data is of 1300m and 1000m, respectively (Fig. 5b, d, f).

Figure 10 shows the results of thermal modelling for the wells in the eastern Adjara-Trialeti FTB (Kumisi 1, Kumisi 2 and Patardzeuli-E1), produced assuming the HF model with a peak around 45 Ma (Fig. 10d), that is the most realistic one taking into account the geological evolution of the Adjara-Trialeti back-arc rift basin (Adamia et al., 1981, 2011; Banks et al., 1997). See Section 5.1.1 for further discussion on the thermal modelling results.

In the two wells (Norio 200 and Satskhenisi 102) from the western Kura Basin a high spread characterises the Tmax data distribution. Nonetheless, a Tmax trend can be recognised along the Maikopian section in the Satskhenisi 102 well; in this well, thermal maturity can be further constrained by means of ten VR_o% data (Fig. 6c, d). Combining Tmax and VR_o% data in the Satskhenisi 102 well, thermal maturity ranges between about 0.4 (at the top of the Maikop section) to about 0.6 (at the bottom of the Maikop section) of equivalent VR_o%. Such trend can be fitted with an additional burial comprised between 800 and 2000 m assuming a constant HF similar to the present-day value, and between 0 and 1300 m assuming the HF model with a peak at around 45 Ma (Fig. 6c and d, respectively). The additional burial considered do not comprise 500m of shales that we assume were deposited during the Sarmatian since they are present in the nearby Norio 200 well (Fig. 3; Table 3). For what concerns the Norio 200 well, the additional burial required to fit thermal maturity data varies between 1000 and 2500 m assuming a constant HF, and between 800 and 2000 m assuming the rifting model with a peak at ~ 45 Ma (Fig. 6a, c).

Figure 11 shows the results of thermal modelling for the wells in the western Kura Basin (Norio 200 and Satskhenisi 102), produced assuming a constant HF of 45 mW/m^2 (Fig. 11c), which is the more realistic scenario given the flexural nature of the Kura foreland basin (Adamia et al., 2010; Nemčok et al., 2013; Patton, 1993). See Section 5.1.2 for further discussion on the thermal modelling results.

4.3 Structural cross-section

The geological cross-section shown in Figure 7 was created linking together three interpreted depth-migrated seismic reflection profiles (lines 1401, 13 and 3004) provided by the Georgian Oil & Gas Company. The cross-section, oriented NE-SW, covers the eastern Adjara-Trialeti FTB and the southernmost western Kura Basin, and depicts the overall structural layout of the study area.

In the section, the Adjara-Trialeti FTB is characterised at depth by mostly north-verging and subordinately south-verging duplex systems made of Cretaceous-Paleogene rocks, which accommodate considerable shortening (Fig. 7). The Teleti and Varketili anticlines, separated by a broad syncline, are fault-propagation folds developed upon south- and north-directed thrusts, respectively, involving the Cretaceous-to-Eocene sequence. Structural interpretation at shallow crustal levels (0-4 km) is consistent with those shown in other published cross-sections and interpreted seismic lines in the study area (c.f. Alania et al., 2021a, 2021c). As seismic resolution decreases at deeper levels, different models can be applied to reconstruct the structural style. For example, Alania et al. (2021a, 2021b) propose an interpretation implying a higher degree of shortening than Tari et al. (2021).

Previous work (Banks et al., 1997; Candaux, 2021; Gusmeo et al., 2021; Sosson et al., 2016; Tari et al., 2018) showed that the overall geometry of the Adjara-Trialeti FTB can be interpreted as the result of the structural inversion of the former extensional faults accommodating back-arc rifting, in agreement with the architecture shown in the shallowest portion of Fig. 7. The complex fault pattern at depth was formed during the progressive northward progradation of the retro-wedge of the Lesser Caucasus (Alania et al., 2021a;

Gusmeo et al., 2021). The Ormoiani syncline is mainly made of Maikopian (Oligocene-Early Miocene) rocks, topped by thin Middle and Upper Miocene rocks.

Since Maikopian rocks are involved in the deformation (Fig. 7), the cross-section indicates that inception of deformation postdates the Early Miocene, a timing in agreement with the Middle Miocene inception of inversion of the Adjara-Trialeti FTB, based on seismic interpretation (Pace et al., 2019) and low-temperature thermochronology results (Gusmeo et al., 2021; this study).

The northern segment of the section shows a series of shallow, thin-skinned south-verging thrusts involving Miocene rocks, which overlie the frontal part of the Adjara-Trialeti FTB (Fig. 7). In this sector, a triangle zone is formed by the interference between the north-verging structures related to the Adjara-Trialeti FTB and the south-directed thrusts deforming the Kura Basin. Further to the west, published seismic lines show a very similar structure in the triangle zone (Alania et al., 2018, 2020, 2021a; Pace et al., 2019; Tari et al., 2021), but there the south-verging thrusts deforming the Kura Basin do not overthrust yet the Adjara-Trialeti FTB (Fig. 12). Since Upper Miocene rocks are clearly involved in the south-verging thrusts, the onset of thin-skinned deformation is not older than Late Miocene (Fig. 7).

5. Discussion

5.1 Thermal and burial histories

The integration of organic thermal indicators, thermochronology and structural data is key in basin analysis and has been successfully applied in a number of studies focused on the burial and erosion history of sedimentary successions (Balestra et al., 2019; Corrado et al., 2020; Di

Paolo et al., 2012; Schito et al., 2018) and/or on the deformation style within an orogenic wedge (Andreucci et al., 2014; Caricchi et al., 2015; Corrado et al., 2021; Curzi et al., 2020; Di Paolo et al., 2012).

The overall evolution of the Adjara-Trialeti FTB and the western Kura Basin has involved different subsidence mechanisms (rifting vs. lithospheric flexure) and complex patterns of structural interference between the facing Greater Caucasus and Adjara-Trialeti fold-and-thrust belt, to the point that only an integrated approach can unravel with sufficient detail the timing and magnitude of maximum burial and exhumation, as well as the paleo-heat flows during basin evolution.

5.1.1 Adjara-Trialeti FTB

In the Adjara-Trialeti FTB low-temperature thermochronologic analyses and inverse modelling of the two surface samples analysed provide an insight into the post-Oligocene thermal history of the basin, while thermal models calibrated by means of wells stratigraphy and thermal maturity data also constrain the oldest phases of burial. Despite the uncertainties related to the high spread of Tmax well data (Fig. 5), the results suggest thermal maturity at the onset and at the peak of the oil window in the Maikop and Late Eocene sections, respectively. In the Patardzeuli-E1 and Kumisi 2 wells, hydrocarbon generation by Eocene and, in minor account, Maikop sources has been confirmed by gas chromatography-mass spectrometry (GC-MS) data (Sachsenhofer et al., 2021), strengthening the reliability of our dataset. Between two HF scenarios tested in the sensitivity analysis (Fig. 5), the one involving a peak of HF during Middle Eocene (around 45 Ma; Fig. 10d) back-arc rifting (Adamia et al., 1977, 1981, 2011; Okrostsvaridze et al., 2018) best suits the geological evolution of the Adjara-Trialeti Basin. Additional support to the tested HF model is provided by the high present-day heat flow in the western sector of the fold-and-thrust belt (Melikadze et al., 2015). In this area, rifting was more pronounced and arguably decreased at a slower pace, thus suggesting that also the easternmost Adjara-Trialeti Basin experienced in the past higher HF values than the present-day value of 50 mW/m^2.

Given that rifting did not lead to continental break-up and oceanization, HF values in the Adjara-Trialeti Basin probably never exceeded 100 mW/m^2, as shown in typical continental rift basins such as the Rhine Graben, Lake Tanganika, Gulf of Suez and Rio Grande Rift (Allen & Allen, 2013; Ebinger et al., 1989; Evans, 1988; Friedmann & Burbank, 1995; Jackson & McKenzie, 1988; Morley et al., 1990; Patton et al., 1994). Considering that our study area in the easternmost Adjara-Trialeti FTB was likely a marginal portion of the basin, a value of 70 mW/m^2 can be reasonably assumed as adequate to represent the maximum HF peak during rifting. Nonetheless, also higher values were tested in a trial-and-error approach, and the results show significant changes only in the deeper part of the maturity curve, which increases its slope and loses fit with the data.

Even with the HF model involving a peak around 45 Ma, an additional burial of about 1 km was still required to fit thermal maturity data (Fig. 5a, c and e). In the Kumisi 1 well such additional burial is slightly higher (1.3 km) to compensate for the missing uppermost part of the Maikop section, which is instead present in the Kumisi 2 well. This 1.0-1.3 km of additional burial can reasonably be attributed to a sedimentary load deposited in the Early Miocene, between about 20 and 15 Ma (Table 3), i.e. after the most recent sedimentary units preserved in the wells and before the cooling event accompanying erosion, that could represent the persistence of marine conditions in the Adjara-Trialeti basin during Burdigalian-Langhian times. Such sedimentary burial matches the fast increase of temperatures detected by statistical inverse modelling of AFT data between Burdigalian and Langhian times (Figs. 8 and 9). Conversely, tectonic loading at that time is unrealistic, since the nearby advancing thrusts deforming the Kura Basin were activated in the Late Miocene (Sarmatian-Pontian; Alania et al., 2017; Nemčok et al., 2013). Finally, the thickness of the Lower Miocene section (1-2 km) shown in the cross-section of Figure 7 supports the interpretation of such additional loading as due to sedimentary burial.

Based on the assumptions described above on the thermal history (i.e. the HF model applied) and the additional sedimentary burial required to fit thermal maturity data, the isotherms derived from thermal modelling of the Adjara-Trialeti wells predict that maximum paleotemperatures experienced by the Maikop section (Oligocene-Early Miocene) in all three wells were comprised between about 90 and 110 °C (Suppl. Mat. Fig. S6). This conclusion agrees with (i) statistical inverse modelling of AFT data (e.g. Figs. 8 and 9), which indicate that Maikop samples from the Adjara-Trialeti FTB are partially reset and hence experienced maximum paleotemperature within the Partial Annealing Zone of apatite, i.e. between 60 and 120 °C (this study; Gusmeo et al., 2021), and (ii) maximum paleotemperatures estimated on Maikop samples from multiple thermal maturity proxies within the Adjara-Trialeti FTB (Corrado et al., 2021).

The only other thermal model available for the study area (Pupp et al., 2018) estimates a total amount of eroded section of ca. 3.5 km, different from our estimates of 1.0-1.3 km. This value results from the very low heat-flow value used as input data: Pupp et al. (2018) used a constant value of 40 mW/m^2 to model a pseudo-well built upon surface data from the Tbilisi area, considered as part of the Kura Basin. Based on geological and geophysical data (see for example Figs. 2 and 7), the section analysed by Pupp et al. (2018) is actually part of the Adjara-Trialeti domain, hence the higher amount of burial derived from an underestimation of the heat flow values. On the other hand, the modelling of Pupp et al. (2018), based on stratigraphy, shows an increase in subsidence rates in the Early Miocene and sets the beginning of exhumation of the studied section at 15 Ma, in agreement with our models (Fig. 10).

According to our thermal modelling results (Fig. 10), the three wells in the eastern Adjara-Trialeti FTB show a similar burial pattern, despite some minor differences in the thickness of equivalent stratigraphic units, in the age range of the sampled sections (e.g. Late Cretaceous-Miocene in Kumisi 1 versus Late Eocene-Miocene in Kumisi 2), and in the maximum depths estimated by the models. The burial history of the Kumisi 1 and Patardzeuli-E1 wells is characterised by rapid subsidence starting in the late Paleocene and continuing, with varying intensity, until the mid-Miocene (Fig. 10). The Eocene-Miocene burial history of the Kumisi 2 well is virtually identical but this borehole did not penetrate the older chronostratigraphic units. Sedimentation rates were higher during the late Paleocene-Early Eocene in the Kumisi 1 and Patardzeuli-E1 wells, and during the Middle-Late Eocene and Early Miocene in all three wells (Fig. 10a, b and c). Timing of inception of cooling/exhumation was set at 15 Ma for all three wells, based on thermochronological data on the beginning of tectonic inversion of the Adjara-Trialeti back-arc basin (Figs. 8 and 10; see Section 4.1; Gusmeo et al., 2021).

5.1.2 Kura Basin

In the western sector of the Kura Basin, the Oligocene portion of the Maikop section was sampled and studied within the Norio 200 and Satskhenisi 102 wells. Despite a large data spread, thermal maturity at the onset of the oil window is also confirmed by GC-MS data (DIG, 2014) and by the datasets reported in Corrado et al. (2021), Pupp et al. (2018) and Sachsenhofer et al. (2021).

During the Oligocene, the western sector of the Kura basin acted as a foreland basin in front of the northward advancing Lesser Caucasus - Adjara-Trialeti system (Nemčok et al., 2013). Given the relatively thick and rigid crust upon which the Kura foreland basin developed (Adamia et al., 2010; Alania et al., 2017; Banks et al., 1997; Nemčok et al., 2013), it could be argued that the heat flow has been relatively low throughout the entire evolution of the basin, as already suggested by Corrado et al. (2021). Thus, even if for the sake of comparison the scenario involving a HF peak around 45 Ma (as in the adjacent Adjara-Trialeti domain) has been tested too (Fig. 6), the constant HF scenario is in our view the most appropriate to apply. Based on the heat-flow map of the Black-Caspian seas region (Kutas, 2010) the present-day heat-flow value in the studied sector of the western Kura Basin is around 45 mW/m^2, a slightly lower value than in the adjacent, relatively hotter, Adjara-Trialeti FTB. Such value agrees with the low geothermal gradient of the area (28 °C/km; Patton, 1993), and is in the range of other foreland basins worldwide (20-60 mW/m^2) (Allen and Allen, 2013; Sachsenhofer, 2001; Weides and Majorowicz, 2014).

Using a steady-state heat-flow model, both wells in the Kura Basin required an additional burial after the deposition of the Sarmatian section (the latest sedimentary succession preserved within the two wells) which ended at about 8 Ma in the Norio 200 well. Given the large spread of Tmax data in both wells, it is not an easy task to accurately determinate the amount of additional burial (Fig. 6a and c). Nevertheless, the maturity curves built assuming 1800 m and 1300 m of additional burial for Norio 200 and Satskhenisi 102, respectively, seem to fit at best the data. Such estimations are just below the range given by Corrado et al. (2021) who, based on surface and subsurface thermal maturity data, calculated 2-3 km of Kura basin fill erosion. It is worth noting that these values can sensibly change depending on the lithologies assumed for the additional loading. In our models, we used a mixed lithology composed of shales and sandstones, which is the same one characterising the Sarmatian sections (Fig. 3, Table 3) and best represents the Miocene sedimentary fill of the Kura Basin.

Thermal modelling of the two wells from the western Kura Basin produced a broadly similar subsidence pattern (Fig. 11). Relatively fast subsidence during the Oligocene was followed by slower rates in the Early-Middle Miocene and very fast burial in the Late Miocene, especially after 8 Ma. This means that the additional burial required to fit thermal maturity data was emplaced very rapidly, suggesting a tectonic origin rather than sedimentary burial: the most probable cause of such tectonic loading is the emplacement of south-verging thrusts (Figs. 1, 2, 7 and 12) related to southward propagation of deformation from the Greater Caucasus.

Since precise constraints on the beginning of cooling/exhumation in this sector are not available, such timing was tentatively set at 6 Ma, i.e. after the most recent deposits within the Norio 200 well (8 Ma; Fig. 11, Table 3). However, after several simulations (with such timing varying between 7 and 3 Ma), we found that differences in the timing of inception of erosion did not affect significatively the results. A latest Miocene-Early Pliocene age of inception of erosion/cooling is also in agreement with the Late Miocene age of the youngest rock units within the thrust sheets imaged in the seismic lines across the southern Kura basin (e.g. Fig. 7) and with previous estimates on the inception of deformation in the Kura Basin (Alania et al., 2017; Nemčok et al., 2013).

According to modelling results, the base of the Oligocene section in both wells experienced maximum paleotemperatures in excess of 80 °C (Fig. 11).

5.2 Tectonic implications

The integration of our new AFT inverse modelling and thermal modelling results constrains the burial/exhumation history of the structurally complex transition zone between two adjacent geologic domains, the Adjara-Trialeti FTB to the south and the Kura Basin to the north, which differ in age, origin, subsidence mechanisms and evolution.

A rift model best describes the HF evolution in the eastern Adjara-Trialeti back-arc basin, with a peak at ca. 70mW/m^2 around 45 Ma followed by gradual reduction down to the present-day value of 50 mW/m^2 (Fig. 10d). Applying such HF model, the Adjara-Trialeti basin experienced continuous subsidence from the Paleocene to the middle Miocene, punctuated by three main pulses of increased subsidence (Fig. 10). High subsidence rates were first registered in the Kumisi 1 and Patardzeuli-E1 wells in the late Paleocene-Early Eocene. During this time a thick succession, including the terrigenous turbidites of the Borjomi Flysch (Adamia et al., 2011; Banks et al., 1997; Yılmaz et al., 2000, 2014), was deposited in the Adjara-Trialeti basin in the northern foreland of the Erzinçan-Sevan-Akera orogen, which was experiencing a gradient of increasing flexural subsidence from west to east (Gusmeo et al., 2021), as confirmed by the progressive eastward thickening of the Borjomi Flysch (Gamkrelidze, 1949; Yılmaz et al., 2000). Interpreting the pre-depositional history of detrital samples as derived from inverse modelling must be done with great care, because of the intrinsic assumptions that are hardly verifiable (Malusà and Fitzgerald, 2020). Nevertheless, our thermochronologic inverse modelling results (Gusmeo et al., 2021; this study) are supported by very high chi-square values (close to 100%) and describe a thermal history (i.e. fast cooling/exhumation of the sediment source area during Paleocene-Eocene times; Figs. 8 and 9) that is compatible with the reconstructed geologic evolution of the region during that time span, when the Northern Neotethys finally closed along the Izmir-Ankara-Erzinçan-Sevan-Akera suture zone due to the oblique collision between the Anatolide-Tauride terrane and the southern Eurasian margin (Barrier et al., 2018; Rolland et al., 2019; Sosson et al., 2010; Stampfli and Hochard, 2009). As a result, the building-up of the Lesser Caucasus (e.g. Barrier et al., 2018; Okay and Tüysüz, 1999; Sosson et al., 2010) was most likely the source of the sediments deposited in the Adjara-Trialeti basin, that was forming under lithospheric flexure due to loading by the Lesser Caucasus retro-wedge (Gamkrelidze, 1949; Gusmeo et al., 2021). During the final stages of closure of the Northern Neotethys, slab roll-back brought, in the Lutetian, to the main phase of continental rifting within the Adjara-Trialeti basin, as testified by the intrusion of plutonic/hypabyssal bodies and by the deposition of volcanic and volcaniclastic rocks (Adamia et al., 2011; Gamkrelidze et al., 2019; Okrostsvaridze et al., 2018). The second phase of increased subsidence rate (Middle-Late Eocene) is likely a consequence of such continental rifting. Furthermore, the presence of volcanic and plutonic rocks, most abundant in the western sector of the basin towards the Black Sea coast, corroborates the hypothesis of high heat-flow at that time (Fig. 10).

The third phase of fast burial (Early Miocene), previously unrecognised, is evident in the thermal models (Fig. 10) and confirmed by the fast heating phase outlined by inverse modelling of AFT data (Figs. 8 and 9). At this time the area was characterized by the convergence between the Greater and Lesser Caucasus (Nemčok et al., 2013). We propose that strike-slip tectonics could have caused such a subsidence pulse just before the uplift of the area, based on (i) paleomagnetic and structural data (Avagyan et al., 2005; Meijers et al., 2015; Rolland, 2017) suggesting oroclinal bending accompanied by strike-slip deformation in the Lesser Caucasus/Transcaucasus during the Cenozoic; (ii) present-day GPS vectors indicating anticlockwise rotation of the Arabian Plate and in the Kura Basin (Forte et al., 2014; Reilinger et al., 2006); (iii) earthquake focal mechanisms suggesting transpression/transtension in the eastern Transcaucasus (Ismail-Zadeh et al., 2020; Sokhadze et al., 2018; Tibaldi et al., 2019); (iv) fault patterns likely associated to the structural inversion of strike-slip (transtensional) faults imaged in seismic profiles in the eastern Adjara-Trialeti fold-and-thrust belt (see cross-section of Fig. 7 and Tari et al., 2021), and (v) the high subsidence rates evidenced in the modelling results (Fig. 10). Additional field-based structural studies are needed to test this hypothesis.

Early to Middle Miocene (20-15 Ma) Adjara-Trialeti basin inversion is constrained by inverse modelling of thermochronologic data (Figs. 8 and 9; Table 1) and confirms previous results obtained more to the west along the orogenic belt (Gusmeo et al., 2021). Exhumation can be framed in the context of the Middle Miocene hard collision between the Arabian and Eurasian plates along the Bitlis-Zagros suture zone (Cavazza et al., 2018; Okay et al., 2010; Rolland et al., 2012) that caused reactivation of tectonic structures, basin inversion, and strike-slip deformation in the hinterland of the collision zone, from the eastern Pontides and the East Anatolian-Iranian Plateau, to the Lesser and Greater Caucasus, to the Talysh and Alborz ranges (Albino et al., 2014; Avagyan et al., 2005; Avdeev and Niemi, 2011; Axen et al., 2001; Ballato et al., 2008, 2016; Barber et al., 2018; Cavazza et al., 2017, 2019; Corrado et al., 2021; Gavillot et al., 2010; Gusmeo et al., 2021; Madanipour et al., 2017; Mosar et al., 2010; Paknia et al., 2021; Vasey et al., 2020; Vincent et al., 2020).

Our preferred model describing the HF evolution in the western Kura Basin assumes a constant HF of 45 mW/m^2 (Fig. 11c) throughout the Oligocene-to-Present basin history. Applying such model, in the western Kura basin the subsidence curves derived from the burial histories of the two analysed wells (Fig. 11) mostly describe the evolution during Maikop deposition and show continuous burial since the Oligocene, with two main pulses of enhanced subsidence in the Oligocene and in the Middle-Late Miocene, respectively.

A first phase of relatively fast subsidence (higher in Satskhenisi 102 than in Norio 200) occurred during the Oligocene (Fig. 11), when the western Kura foreland basin behaved as a flexural basin, reacting by prominent fill asymmetry to loading by the northward advancing Lesser Caucasus - Adjara-Trialeti system (Nemčok et al., 2013). It was only in the Middle-Late Miocene that the flexural wave induced by the south-verging advancement of the Greater Caucasus structural front reached the southern margin of the Kura Basin (Figs. 11 and 12). The sedimentation pattern at that time is typical of foreland basins, characterized by convex-upward subsidence curves (e.g. Allen and Allen, 2013; Fig. 11).

Competing and asymmetrical episodes of flexural subsidence within the western Kura Basin have been envisioned by Nemčok et al. (2013), who interpreted the marked southward thickening of the Oligocene section and the northward thickening of the Early-Middle Miocene one as effects of flexural loading by the advancing Lesser Caucasus and Greater Caucasus, respectively.

Finally, in Late Miocene times (late Sarmatian-Pontian; Alania et al., 2017; Nemčok et al., 2013) the southward propagation of deformation from the Greater Caucasus affected the Kura Basin in the area of the Norio 200 and Satskhenisi 102 wells (Fig. 12). This resulted in the emplacement of a complex system of thin-skinned south-verging thrusts, arguably responsible for the additional 1.3-1.8 km of tectonic loading required to fit thermal maturity data (Figs. 11 and 12). After this fast burial, which led to maximum paleo-temperatures of more than 80°C at the bottom of the succession, the area was ultimately exhumed and experienced significant erosion. The complex deformation that took place in the southern part of the Kura foreland basin is represented by deformation and uplift of Miocene strata by thin-skinned thrusting at the top of the triangle zone (Fig. 7). Such a structural thickening induced the erosion of a ca. 1.3-1.8 km thick section since latest Miocene-Pliocene times.

The overall tectonic evolution and burial-exhumation history reconstructed for the Adjara-Trialeti and Kura basins, in the central Transcaucasian sector, can be framed in the context of the broad Arabia-Eurasia collision zone. Initial flexural subsidence and subsequent back-arc rifting in the Adjara-Trialeti Basin can be interpreted as a consequence of continental collision along the Erzinçan-Sevan-Akera suture during Paleocene-Early Eocene times and roll-back during the Middle Eocene, respectively. During the Oligocene, thermal subsidence was affecting the Adjara-Trialeti basin (Fig. 10), whereas the Kura Basin was flexured by the advance of the Lesser Caucasus system (Fig.11). The Middle Miocene inception of inversion of the Adjara-Trialeti basin defined in this study and in Gusmeo et al. (2021), as well as the timing of renewal of flexural behaviour in the Kura Basin highlighted by thermal modelling results (Fig. 11), can both be ascribed to far-field stress propagation from the Bitlis-Zagros suture zone, hundreds of kilometres to the south, where the Middle Miocene hard collision between the Arabian and Eurasian plates took place (Cavazza et al., 2018; Okay et al., 2010). Furthermore, continued northward stress transmission may have been also responsible for shortening/uplift in the Greater Caucasus. Given that in its central sector this orogen is mainly south-verging (Forte et al., 2014), far-field stress transmission from the Bitlis-Zagros suture zone could ultimately be responsible for southward propagation of deformation from the Greater Caucasus, affecting also the Kura Basin (Fig. 12). Such a stress field is active also at present in the Transcaucasus, as demonstrated by GPS and earthquakes data (Karakhanyan et al., 2013; Reilinger et al., 2006; Sokhadze et al., 2018; Tsereteli et al., 2016).

6. Conclusions

In this paper we apply an integrated approach to the study of the complex transition zone between the eastern Adjara-Trialeti FTB and the western Kura Basin (central Georgia). The combination of AFT inverse modelling, well thermal modelling and seismic interpretation has elucidated the pattern of subsidence/exhumation and has provided new constraints on the overall tectonic evolution of the eastern Georgian sector of the Transcaucasus.

New AFT inverse modelling results from the eastern Adjara-Trialeti FTB indicate latest Paleocene-Early Eocene fast cooling/exhumation, arguably linked with final closure of the Northern Neotethys ocean and subsequent building of the Lesser Caucasus. A previously unrecognized and localized Early Miocene phase of fast subsidence and heating is tentatively attributed to strike-slip motion components between the Greater and Lesser Caucasus orogenic systems. AFT modelling results also confirms the mid-Miocene inception of structural inversion of the Adjara-Trialeti basin.

Thermal modelling of the Adjara-Trialeti inverted back-arc basin delineates three pulses of enhanced subsidence in Late Paleocene-Early Eocene, Middle-Late Eocene and Early Miocene times in the Adjara-Trialeti basin, associated respectively to flexural subsidence, rifting and strike-slip tectonics. Modelling results also predict that about 1.0-1.3 km of sedimentary rocks have been eroded since inversion started.

Best-fit thermal models from the Kura Basin describe a complex subsidence pattern during Oligocene-Miocene times, resulting from the interference between the competing and oppositely advancing Lesser and Greater Caucasus orogenic systems. During the Late Miocene the southwestern Kura Basin experienced rapid tectonic burial (ca. 1.3-1.8 km), related to south-verging thrusts linked to southward propagation of deformation from the Greater Caucasus, ultimately followed by exhumation and erosion.

On a larger scale, the tectonic evolution and burial/exhumation history of central Transcaucasia can be correlated with episodic continental accretion along the Eurasian plate margin related to (i) collision of the Anatolide-Tauride terrane and the ensuing development of the Erzinçan-Sevan-Akera suture in the latest Cretaceous - Eocene, and (ii) the hard collision of Arabia along the Bitlis-Zagros suture zone in the Miocene.

Acknowledgements

We thank GOGC (Georgian Oil & Gas company) for kindly providing part of the lithological and thermal maturity data used in this study. Platte River Associates, Inc. is acknowledged for providing an academic licence for the Basin Mod 2-D software package. Reinhard Sachsenhofer (Montanuniversität Leoben) provided useful comments on an earlier version of the manuscript. We thank JAES Associate Editor Michel Faure and an anonymous reviewer for their constructive input. Irene Albino assisted in sample preparation for fission-track analysis. This research was funded by the PRIN Program of the Italian Ministry of University and Research 2017-2020.

References

Abdullah, W.H., Togunwa, O.S., Makeen, Y.M., Hakimi, M.H., Mustapha, K.A., Baharuddin, M.H., Sia, S.G., Tongkul, F., 2017. Hydrocarbon source potential of Eocene-Miocene sequence of Western Sabah, Malaysia. Mar. Pet. Geol. 83, 345–361. https://doi.org/10.1016/j.marpetgeo.2017.02.031

Adamia, S.A., Akhvlediani, K.T., Kilasonia, V.M., Nairn, A.E.M., Papava, D., Patton, D.K., 1992. Geology of the republic of Georgia: a review. Int. Geol. Rev. 34, 447–476.

Adamia, S.A., Alania, V., Chabukiani, A., Chichua, G., Enukidze, O., Sadradze, N., 2010. Evolution of the Late Cenozoic basins of Georgia (SW Caucasus): a review, in: Sosson, M., Kaymakci, N., Stephenson, R.A., Bergerat, F., Starostenko, V. (Eds.), Sedimentary Basin Tectonics from the Black Sea and Caucasus to the Arabian Platform. Geological Society, London, Special Pubblications, 340, pp. 239–259.

Adamia, S.A., Chkhotua, T., Kekelia, M., Lordkipanidze, M., Shavishvili, I., Zakariadze, G., 1981. Tectonics of the Caucasus and adjoining regions: implications for the evolution of the Tethys ocean. J. Struct. Geol. 3, 437–447. https://doi.org/https://doi.org/10.1016/0191-8141(81)90043-2

Adamia, S.A., Chkhotua, T.G., Gavtadze, T.T., Lebanidze, Z.A., Lursmanashvili, N.D., Sadradze, N.G., Zakaraia, D.P., Zakariadze, G.S., 2017. Tectonic setting of Georgia-Eastern Black Sea: A review, in: Sosson, M., Stephenson, R.A., Adamia, S.A. (Eds.), Tectonic Evolution of the Eastern Black Sea and Caucasus. Geological Society, London, Special Publications 428, pp. 11–40. https://doi.org/10.1144/SP428.6

Adamia, S.A., Lordkipanidze, M.B., Zakariadze, G.S., 1977. Evolution of an active continental margin as exemplified by the Alpine history of the Caucasus. Tectonophysics 40, 183–199. https://doi.org/https://doi.org/10.1016/0040-1951(77)90065-8

Adamia, S.A., Zakariadze, G., Chkhotua, T., Sadradze, N., Tsereteli, N., Chabukiani, A., Gventsadze, A., 2011. Geology of the Caucasus: A Review. Turkish J. Earth Sci. 20, 489–544. https://doi.org/10.3906/yer-1005-11

Alania, V., Beridze, T., Enukidze, O., Chagelishvili, R., Lebanidze, Z., Maqadze, D., 2021a. The Geometry of the two orogens convergence and collision zones in central Georgia: new data from seismic reflection profiles, in: Bonali, F.L., Pasquarè Mariotto, F.A., Tsereteli, N. (Eds.), Building Knowledge for Geohazard Assesment and Management in the Caucasus and Other Regions. Springer, Dordrecht, pp. 73–88.

Alania, V., Beridze, T., Enukidze, O., Lebanidze, Z., Razmadze, A., Sadradze, N., Tevzadze, N., 2020. Structural model of the frontal part of the eastern Achara-Trialeti fold-and-thrust belt: The results of seismic profile interpretation. Bull. Georg. Natl. Acad. Sci. 14, 62–68.

Alania, V., Chabukiani, A.O., Chagelishvili, R.L., Enukidze, O. V., Gogrichiani, K.O., Razmadze, A.N., Tsereteli, N.S., 2017. Growth structures, piggy-back basins and growth strata of the Georgian part of the Kura foreland fold–thrust belt: implications for Late Alpine kinematic evolution, in: Sosson, M., Stephenson, R.A., Adamia, S.A. (Eds.), Tectonic Evolution of the Eastern Black Sea and Caucasus. Geological Society, London, Special Publications 428, pp. 428–445. https://doi.org/10.1177/1010539510370992

Alania, V., Enukidze, O., Glonti, N., Razmadze, A., Chabukiani, A., Giorgadze, A., Vakhtang Glonti, B., Koiava, K., Beridze, T., Khutsishvili, S., Chagelishvili, R., 2018. Structural Architecture of the Kura Foreland Fold-and-thrust Belt Using Seismic Reflection Profile, Georgia. Univers. J. Geosci. 6, 184–190. https://doi.org/10.13189/ujg.2018.060402

Alania, V., Kvavadze, N., Enukidze, O., Beridze, T., Gventsadze, A., Tevzadze, N., 2021b. Seismic interpretation of southern part of the eastern Achara-Trialeti fold-and-thrust belt, Georgia. Bull. Georg. Natl. Acad. Sci. 15, 57–62.

Alania, V., Pace, P., Corrado, S., Gusmeo, T., Beridze, T., Sadradze, N., Tevzadze, N., 2021c. Preliminary Structural Interpretation of a Seismic Profile across the Frontal Sector of the Eastern Achara-Trialeti Fold-and-Thrust Belt. Bull. Georg. Natl. Acad. Sci. 15, 74–80.

Alavi, M., 1994. Tectonics of the Zagros orogenic belt of Iran: new data and interpretations. Tectonophysics 229, 211–238.

Albino, I., Cavazza, W., Zattin, M., Okay, A.I., Adamia, S.A., Sadradze, N., 2014. Far-field tectonic effects of the Arabia–Eurasia collision and the inception of the North Anatolian Fault system. Geol. Mag. 151, 372–379. https://doi.org/10.1017/s0016756813000952

Allen, P.A., Allen, J.R., 2013. Basin Analysis: Principles and Application to Petroleum Play Assessment, Science. https://doi.org/10.1126/science.208.4442.393

Andreucci, B., Castelluccio, A., Corrado, S., Jankowski, L., Mazzoli, S., Szaniawski, R., Zattin, M., 2014. Interplay between the thermal evolution of an orogenic wedge and its retro-wedge basin: An example from the Ukrainian Carpathians. Bull. Geol. Soc. Am. 127, 410–427. https://doi.org/10.1130/B31067.1

Avagyan, A., Sosson, M., Philip, H., Karakhanian, A., Rolland, Y., Melkonyan, R., Reba, S., Davtyan, V., 2005. Nogene to Quaternary stress field evolution in Lesser Caucasus and adjacent regions using fault kinematics analysis and volcanic cluster data. Geodin. Acta

18, 401–416.

Avdeev, B., Niemi, N.A., 2011. Rapid Pliocene exhumation of the central Greater Caucasus constrained by low-temperature thermochronometry. Tectonics 30, 1–16. https://doi.org/10.1029/2010TC002808

Axen, G.J., Lam, P.S., Grove, M., Stockli, D.F., Hassanzadeh, J., 2001. Exhumation of the west-central Alborz Mountains, Iran, Caspian subsidence, and collision-related tectonics. Geology 29, 559–562. https://doi.org/10.1130/0091-7613(2001)029<0559:EOTWCA>2.0.CO;2

Balestra, M., Corrado, S., Aldega, L., Morticelli, M.G., Sulli, A., Rudkiewicz, J.L., Sassi, W., 2019. Thermal and structural modeling of the Scillato wedge-top basin source-to-sink system: Insights into the Sicilian fold-and-thrust belt evolution (Italy). Bull. Geol. Soc. Am. 131, 1763–1782. https://doi.org/10.1130/B35078.1

Ballato, P., Cifelli, F., Heidarzadeh, G., Ghassemi, M.R., Wickert, A.D., Hassanzadeh, J., Dupont-Nivet, G., Balling, P., Sudo, M., Zeilinger, G., Schmitt, A.K., Mattei, M., Strecker, M.R., 2016. Tectono-sedimentary evolution of the northern Iranian Plateau: insights from middle–late Miocene foreland-basin deposits. Basin Res. 29, 417–446. https://doi.org/10.1111/bre.12180

Ballato, P., Nowaczyk, N.R., Landgraf, A., Strecker, M.R., Friedrich, A., Tabatabaei, S.H., 2008. Tectonic control on sedimentary facies pattern and sediment accumulation rates in the Miocene foreland basin of the southern Alborz mountains, northern Iran. Tectonics 27, 1–20. https://doi.org/10.1029/2008TC002278

Banks, C.J., Robinson, A.G., Williams, M.P., 1997. Structure and regional tectonics of the Achara-Trialeti fold belt and the adjacent Rioni and Kartli foreland basins, Republic of Georgia, in: Robinson, A.G. (Ed.), Regional and Petroleum Geology of the Blacks Sea and Surrounding Region: AAPG Memoirs 68. Tulsa, Oklahoma, pp. 331–346.

Barber, D.E., Stockli, D.F., Horton, B.K., Koshnaw, R.I., 2018. Cenozoic exhumation and foreland basin evolution of the Zagros orogen during the Arabia-Eurasia collision, Western Iran. Tectonics 37, 4396–4420. https://doi.org/10.1029/2018TC005328

Barrier, E., Vrielynck, B., Brouillet, J.F., Brunet, M.-F., (Contributors: Angiolini L., Kaveh F., Poisson A., Pourteau A., Plunder A., Robertson A., Shekawat R., Sosson M., Zanchi, A.., 2018. Paleotectonic reconstruction of the central Tethyan realm. Tectonono-sedimentary-palinspastic maps from late Permian to Pliocene. CCGM/CGMW, Paris.

Behar, F., Beaumont, V., De B. Penteado, H.L., 2001. Rock-Eval 6 Technology: Performances and Developments. Oil Gas Sci. Technol. 56, 111–134. https://doi.org/10.2516/ogst:2001013

Bertrand, R., Lavoie, V., Malo, M., 2010. Maturité thermique et potentiel roche-mère des roches ordoviciennes à dévoniennes du secteur Matapédia–Témiscouata du Bas-Saint-Laurent, Québec. Geol. Surv. Canada, Open File 6576 183.

Boote, D.R.D., Sachsenhofer, R.F., Tari, G., Arbouille, D., 2018. Petroleum Provinces of the Paratethyan Region. J. Pet. Geol. 41, 247–297. https://doi.org/10.1111/jpg.12703

Borrego, A.G., Cook, A., 2017. Sampling and Sample Preparation for Reflected Light Microscopy, in: 10th ICCP Training Course on Dispersed Organic Matter Integrating Transmitted and Reflected Light Microscopy (Instruction Notes). pp. 21–28.

Burnham, A.K., Sweeney, J.J., 1989. A chemical kinetic model of vitrinite maturation and reflectance. Geochim. Cosmochim. Acta 53, 2649–2657. https://doi.org/10.1016/0016-7037(89)90136-1

Butler, R.W.H., 1991. Hydrocarbon maturation, migration and tectonic loading in the Western Alpine foreland thrust belt, in: England, W.A., Fleet, A.J. (Eds.), Petroleum Migration. Geological Society, London, Special Publications 59, pp. 227–244.

Butler, R.W.H., Bond, C.E., Cooper, M.A., Watkins, H., 2018. Interpreting structural geometry in fold-thrust belts: Why style matters. J. Struct. Geol. 114, 251–273. https://doi.org/10.1016/j.jsg.2018.06.019

Candaux, Z.C., 2021. Surface and subsurface structures of the Greater Caucasus flexural basin in Georgia, reconstruction of its tectonic inversion since the Early Cretaceous. Université Cote d'Azur.

Caricchi, C., Aldega, L., Corrado, S., 2015. Reconstruction of maximum burial along the Northern Apennines thrust wedge (Italy) by indicators of thermal exposure and modeling. Bull. Geol. Soc. Am. 127, 428–442. https://doi.org/10.1130/B30947.1

Cavazza, W., Albino, I., Galoyan, G., Zattin, M., Cattò, S., 2019. Continental accretion and incremental deformation in the thermochronologic evolution of the Lesser Caucasus. Geosci. Front. 10, 2189–2202. https://doi.org/10.1016/j.gsf.2019.02.007

Cavazza, W., Albino, I., Zattin, M., Galoyan, G., Imamverdiyev, N., Melkonyan, R., 2017. Thermochronometric evidence for Miocene tectonic reactivation of the Sevan-Akera suture zone (Lesser Caucasus): A far-field tectonic effect of the Arabia-Eurasia collision?, in: Sosson, M., Stephenson, R.A., Adamia, S.A. (Eds.), Tectonic Evolution of the Eastern Black Sea and Caucasus. Geological Society, London, Special Publications 428, pp. 187–198. https://doi.org/10.1144/SP428.4

Cavazza, W., Cattò, S., Zattin, M., Okay, A.I., Reiners, P., 2018. Thermochronology of the Miocene Arabia-Eurasia collision zone of southeastern Turkey. Geosphere 14, 2277–2293. https://doi.org/10.1130/GES01637.1

Cohen, K.M., Finney, S.C., Gibbard, P.L., Fan, J.-X., 2021. The ICS International Chronostratigraphic Chart. Episodes 36, 199–204.

Corrado, S., Gusmeo, T., Schito, A., Alania, V., Enukidze, O., Conventi, E., Cavazza, W., 2021. Validating far-field deformation styles from the Adjara-Trialeti fold-and-thrust belt to the Greater Caucasus (Georgia) through multi-proxy thermal maturity datasets.

Mar. Pet. Geol. 130. https://doi.org/10.1016/j.marpetgeo.2021.105141

Corrado, S., Schito, A., Romano, C., Grigo, D., Poe, B.T., Aldega, L., Caricchi, C., Di Paolo, L., Zattin, M., 2020. An integrated platform for thermal maturity assessment of polyphase, long-lasting sedimentary basins, from classical to brand-new thermal parameters and models: An example from the on-shore Baltic Basin (Poland). Mar. Pet. Geol. 122, 104547. https://doi.org/10.1016/j.marpetgeo.2020.104547

Curzi, M., Aldega, L., Bernasconi, S.M., Berra, F., Billi, A., Boschi, C., Franchini, S., Van der Lelij, R., Viola, G., Carminati, E., 2020. Architecture and evolution of an extensionally-inverted thrust (Mt. Tancia Thrust, Central Apennines): Geological, structural, geochemical, and K–Ar geochronological constraints. J. Struct. Geol. 136. https://doi.org/10.1016/j.jsg.2020.104059

Dewey, J.F., Hempton, M.R., Kidd, W.S.F., Saroglu, F., Şengör, A.M.C., 1986. Shortening of continental lithosphere: the neotectonics of Eastern Anatolia — a young collision zone, in: Coward, M.P., Ries, A.C. (Eds.), Collision. Geological Society, London, Special Publications 19, pp. 1–36. https://doi.org/10.1144/GSL.SP.1986.019.01.01

Di Paolo, L., Aldega, L., Corrado, S., Mastalerz, M., 2012. Maximum burial and unroofing of Mt. Judica recess area in Sicily: ®mplication for the Apenninic-Maghrebian wedge dynamics. Tectonophysics 530–531, 193–207. https://doi.org/10.1016/j.tecto.2011.12.020

DIG, 2014. Sackhenisi #102 Geochemical Analysis. Boulder, CO, United States.

Donelick, R.A., Ketcham, R.A., Carlson, W.D., 1999. Variability of apatite fission-track annealing kinetics: II. Crystallographic orientation effects. Am. Mineral. 84, 1224–1234. https://doi.org/10.2138/am-1999-0902

Donelick, R.A., O'Sullivan, P.B., Ketcham, R.A., 2005. Apatite Fission-Track Analysis. Rev. Mineral. Geochemistry 58, 49–94. https://doi.org/10.2138/rmg.2005.58.3

Dow, W.G., 1977. Kerogen studies and geological interpretations. J. Geochemical Explor. 7, 79–99.

Ebinger, C.J., Bechtel, T.D., Forsyth, D.W., Bow, C.O., 1989. Effective elastic plate thickness beneath the East African and Afar plateaus and dynamic compensation of the uplifts. J. Geophys. Res. B Solid Earth 94, 2883–2901.

Evans, A.L., 1988. Neogene tectonic and stratigraphic events in the Gulf of Suez rift area, Egypt. Tectonophysics 153, 235–247. https://doi.org/10.1016/0040-1951(88)90018-2

Flowers, R.M., Farley, K.A., Ketcham, R.A., 2015. A reporting protocol for thermochronologic modeling illustrated with data from the Grand Canyon. Earth Planet. Sci. Lett. 432, 425–435. https://doi.org/10.1016/j.epsl.2015.09.053

Forte, A.M., Cowgill, E., Murtuzayev, I., Kangarli, T., Stoica, M., 2013. Structural geometries and magnitude of shortening in the eastern Kura fold-thrust belt, Azerbaijan: Implications for the development of the Greater Caucasus Mountains. Tectonics 32, 688–717. https://doi.org/10.1002/tect.20032

Forte, A.M., Cowgill, E., Whipple, K.X., 2014. Transition from a singly vergent to doubly vergent wedge in a young orogen: The Greater Caucasus. Tectonics 33, 2077–2101. https://doi.org/10.1002/2014TC003651

Friedmann, S.J., Burbank, D.W., 1995. Rift basins and supradetachment basins: Intracontinental extensional end-members. Basin Res. 7, 109–127. https://doi.org/10.1111/j.1365-2117.1995.tb00099.x

Galbraith, R.F., 1981. On statistical models for fission track counts. J. Int. Assoc. Math. Geol. 13, 471–478. https://doi.org/10.1007/BF01034498

Gamkrelidze, I., Okrostsvaridze, A., Maisadze, F., Basheleishvili, L., Boichenko, G., 2019. Main features of geological structure and geotourism potential of Georgia, the Caucasus. Mod. Environ. Sci. Eng. 5, 422–442. https://doi.org/10.15341/mese(2333-

2581)/05.05.2019/010

Gamkrelidze, P., 1949. Geological structure of the Adjara-Trialetian folded system. Academy of Sciences of Georgia Press, Tbilisi.

Gavillot, Y., Axen, G.J., Stockli, D.F., Horton, B.K., Fakhari, M.D., 2010. Timing of thrust activity in the High Zagros fold-thrust belt, Iran, from (U-Th)/He thermochronometry. Tectonics 29. https://doi.org/10.1029/2009TC002484

Gleadow, A.J.W., Duddy, I.R., 1981. A natural long-term track annealing experiment for apatite. Nucl. Tracks 5, 169–174.

Gleadow, A.J.W., Duddy, I.R., Green, P.F., Lovering, J.F., 1986. Confined fission track lengths in apatite: a diagnostic tool for thermal history analysis. Contrib. to Mineral. Petrol. 94, 405–415.

Gusmeo, T., Cavazza, W., Alania, V.M., Enukidze, O. V, Zattin, M., Corrado, S., 2021. Structural inversion of back-arc basins – The Neogene Adjara-Trialeti fold-and-thrust belt (SW Georgia) as a far-field effect of the Arabia-Eurasia collision. Tectonophysics 803. https://doi.org/10.1016/j.tecto.2020.228702

Hunt, J.M., 1996. Petroleum Geochemistry and Geology. W. H. Freeman and Company, New York.

Ismail-Zadeh, A., Adamia, S.A., Chabukiani, A., Chelidze, T., Cloetingh, S., Floyd, M., Gorshkov, A., Gvishiani, A., Ismail-Zadeh, T., Kaban, M.K., Kadirov, F., Karapetyan, J., Kangarli, T., Kiria, J., Koulakov, I., Mosar, J., Mumladze, T., Müller, B., Sadradze, N., Safarov, R., Schilling, F., Soloviev, A., 2020. Geodynamics, seismicity, and seismic hazards of the Caucasus. Earth-Science Rev. 207. https://doi.org/10.1016/j.earscirev.2020.103222

Jackson, J., McKenzie, D., 1988. The relationship between plate motions and seismic moment tensors, and the rates of active deformation in the Mediterranean and Middle

East. Geophys. J. 93, 45–73. https://doi.org/10.1111/j.1365-246X.1988.tb01387.x

Jarvie, D.M., Claxton, B.L., Henk, F., Breyer, J.T., 2001. Oil and shale gas from the Barnett Shale, Ft . Worth Basin, Texas, in: AAPG National Convention. AAPG Bulletin, Denver, CO, United States.

Jolivet, L., Faccenna, C., 2000. Mediterranean extension and the Africa-Eurasia collision Laurent. Tectonics 19, 1095–1106. https://doi.org/10.1029/2000TC900018

Karakhanyan, A., Vernant, P., Doerflinger, E., Avagyan, A., Philip, H., Aslanyan, R., Champollion, C., Arakelyan, S., Collard, P., Baghdasaryan, H., Peyret, M., Davtyan, V., Calais, E., Masson, F., 2013. GPS constraints on continental deformation in the Armenian region and Lesser Caucasus. Tectonophysics 592, 39–45. https://doi.org/10.1016/j.tecto.2013.02.002

Ketcham, R.A., 2005. Forward and inverse modeling of low-temperature thermochronometry data. Rev. Mineral. Geochemistry 58, 275–314. https://doi.org/10.2138/rmg.2005.58.11

Ketcham, R.A., Carter, A., Donelick, R.A., Barbarand, J., Hurford, A.J., 2007. Improved modeling of fission-track annealing in apatite. Am. Mineral. 92, 799–810. https://doi.org/10.2138/am.2007.2281

Ketcham, R.A., Donelick, R.A., Carlson, W.D., 1999. Variability of apatite fission-track annealing kinetics: III. Extrapolation to geological time scales. Am. Mineral. 84, 1235–1255. https://doi.org/Doi 10.2138/Am.2006.464

Korelskiy, E., Yildiz, T.T., Urazaliev, J., Goloborodko, A., Orlov, A., Tirumanapali, S., Savinov, R., Akhmetov, M., Ivanov, R., 2019. Multidisciplinary engineering approach and proper planning enables successful drilling of one of the deepest exploration HPHT well in the Samgori-Patardzeuli area, Georgia, in: Society of Petroleum Engineers - SPE Russian Petroleum Technology Conference. Moscow, Russia, October 2019. Moscow, Russia, pp. 1–21. https://doi.org/10.2118/196806-ru

Kutas, R.I., 2010. Heat Flow in the Caspian – Black Sea Region and its Tectonic Implications, in: AAPG European Region Annual Conference. Kiev, Ukraine, October 17-19, 2010.

Langford, F.F., Blanc-Velleron, M.M., 1990. Interpreting Rock-Eval Pyrolysis data using graphs of pyrolizable hydrocarbons vs Total Organic Carbon. Am. Assoc. Pet. Geol. Bullettin 74, 799–804.

Lazarev, S., Jorissen, E.L., van de Velde, S., Rausch, L., Stoica, M., Wesselingh, F.P., Van Baak, C.G.C., Yanina, T.A., Aliyeva, E., Krijgsman, W., 2019. Magneto-biostratigraphic age constraints on the palaeoenvironmental evolution of the South Caspian basin during the Early-Middle Pleistocene (Kura basin, Azerbaijan). Quat. Sci. Rev. 222, 105895. https://doi.org/10.1016/j.quascirev.2019.105895

Lordkipanidze, M.B., Meliksetian, B., Djarbashian, R., 1989. Meosozic-Cenozoic magmatic evolution of the Pontian-Crimean-Caucasian region. IGCP Proj. 198 103–124.

Madanipour, S., Ehlers, T.A., Yassaghi, A., Enkelmann, E., 2017. Accelerated middle Miocene exhumation of the Talesh Mountains constrained by U-Th/He thermochronometry: Evidence for the Arabia-Eurasia collision in the NW Iranian Plateau. Tectonics 36, 1538–1561. https://doi.org/10.1002/2016TC004291

Malusà, M.G., Fitzgerald, P.G., 2020. The geologic interpretation of the detrital thermochronology record within a stratigraphic framework, with examples from the European Alps, Taiwan and the Himalayas. Earth-Science Rev. 201. https://doi.org/10.1016/j.earscirev.2019.103074

McKenzie, D., 1978. Some remarks on the development of sedimentary basins. Earth Planet. Sci. Lett. 40, 25–32.

Meijers, M.J.M., Smith, B., Pastor-Galàn, D., Degenaar, R., Sadradze, N., Adamia, S.A., Sahakyan, L., Avagyan, A., Sosson, M., Rolland, Y., Langereis, C.G., Muller, C., 2015.

Progressive orocline formation in the Eastern Pontides – Lesser Caucasus, in: Sosson, M., Stephenson, R.A., Adamia, S.A. (Eds.), Tectonic Evolution of the Eastern Black Sea and Caucasus. Geological Society, London, Special Publications 428. https://doi.org/10.1144/SP428.8

Melikadze, G., Vardigoreli, O., Kapandze, N., 2015. Country Update from Georgia, in: Proceeding World Geothermal Congress 2015. Melbourne, Australia, pp. 1015–1018.

Morley, C.K., Nelson, R.A., Patton, T.L., Munn, S.G., 1990. Transfer Zones in the East African Rift System and their relevance to hydrocarbon exploration in rifts. Am. Assoc. Pet. Geol. Bull. 74, 1234–1253.

Mosar, J., Kangarli, T., Bochud, M., Glasmacher, U.A., Rast, A., Brunet, M.-F., Sosson, M., 2010. Cenozoic-Recent tectonics and uplift in the Greater Caucasus: a perspective from Azerbaijan, in: Sosson, M., Kaymakci, N., Stephenson, R.A., Bergerat, F., Starostenko, V. (Eds.), Sedimentary Basin Tectonics from the Black Sea and Caucasus to the Arabian Platform. Geological Society, London, Special Publications 340, pp. 261–280. https://doi.org/10.1144/SP340.12

Motavalli-Anbaran, S.H., Zeyen, H., Jamasb, A., 2016. 3D crustal and lithospheric model of the Arabia-Eurasia collision zone. J. Asian Earth Sci. 122, 158–167. https://doi.org/10.1016/j.jseaes.2016.03.012

Nemčok, M., Glonti, B., Yukler, A., Marton, B., 2013. Development history of the foreland plate trapped between two converging orogens; Kura Valley, Georgia, case study, in: Nemčok, M., Mora, A., Cosgrove, J.W. (Eds.), Thick-Skin-Dominated Orogens: From Initial Inversion to Full Accretion. Geological Society, London, Special Publications 377, pp. 159–188. https://doi.org/10.1144/SP377.9

Neubauer, T.A., Harzhauser, M., Kroh, A., Georgopoulou, E., Mandic, O., 2015. A gastropod-based biogeographic scheme for the European Neogene freshwater systems.

Earth Sci. Rev. 143, 98–116. https://doi.org/10.1016/j.earscirev.2015.01.010

Okay, A.I., Tüysüz, O., 1999. Tethyan sutures of northern Turkey, in: Durand, B., Jolivet, L., Horváth, F., Séranne, Mi. (Eds.), The Mediterranean Basins: Tertiary Extension within the Alpine Orogen. Geological Society of London, Special Publications 156, pp. 475–515. https://doi.org/10.1144/gsl.sp.1999.156.01.22

Okay, A.I., Zattin, M., Cavazza, W., 2010. Apatite fission-track data for the Miocene Arabia-Eurasia collision. Geology 38, 35–38. https://doi.org/10.1130/G30234.1

Okrostsvaridze, A., Chung, S.L., Chang, Y.H., Gagnidze, N., Boichenko, G., Gogoladze, S., 2018. Zircons U-Pb geochronology of the ore-bearing plutons of Adjara-Trialeti folded zone, Lesser Caucasus and analysis of the magmatic processes. Bull. Georg. Natl. Acad. Sci. 12, 90–99.

Pace, P., Riva, A., Ricciato, A., Tevzadze, R., Janiashvili, A., Sanishvili, A., Alania, V., Enikidze, O., 2019. The Control of Pre-Existing Faults on the Development of Thrust-Related Folds in the Kura Foreland Fold-and-Thrust Belt (Norio License Block, Onshore Georgia), in: AAPG European Region Annual Conference, Paratethys Petroleum Systems Between Central Europe and the Caspian Region. Vienna, Austria, p. March 26-27.

Paknia, M., Ballato, P., Heidarzadeh, G., Cifelli, F., Hassanzadeh, J., Vezzoli, G., Mirzaie Ataabadi, M., Ghassemi, M.R., Mattei, M., 2021. Neogene Tectono-Stratigraphic Evolution of the Intermontane Tarom Basin: Insights Into Basin Filling and Plateau Building Processes Along the Northern Margin of the Iranian Plateau (Arabia-Eurasia Collision Zone). Tectonics 40, 1–36. https://doi.org/10.1029/2020TC006254

Pape, T., Blumenberg, M., Reitz, A., Scheeder, G., Schmidt, M., Haeckel, M., Blinova, V.N., Ivanov, M.K., Sahling, H., Wallmann, K., Bohrmann, G., 2021. Oil and gas seepage offshore Georgia (Black Sea) – Geochemical evidences for a Paleogene-Neogene hydrocarbon source rock. Mar. Pet. Geol. 128. https://doi.org/10.1016/j.marpetgeo.2021.104995

Patton, D.K., 1993. Samgori Field, Republic of Georgia: Critical Review of Island-Arc Oil and Gas. J. Pet. Geol. 16, 153–167. https://doi.org/10.1111/j.1747-5457.1993.tb00103.x

Patton, T.L., Moustafa, A.R., Nelson, R.A., Abdine, S.A., 1994. Tectonic Evolution and Structural Setting of the Suez Rift: Chapter 1: Part I. Type Basin: Gulf of Suez, in: Landon, S.M., Coury, A.B. (Eds.), Interior Rift Basins. AAPG Memoir 59, pp. 9–55. https://doi.org/10.1306/M59582

Pupp, M., Bechtel, A., Ćorić, S., Gratzer, R., Rustamov, J., Sachsenhofer, R.F., 2018. Eocene and Oligo-Miocene source rocks in the Rioni and Kura Basins of Georgia: depositional environment and petroleum potential. J. Pet. Geol. 41, 367–392. https://doi.org/10.1111/jpg.12708

Reilinger, R., McClusky, S., Vernant, P., Lawrence, S., Ergintav, S., Cakmak, R., Ozener, H., Kadirov, F., Guliev, I., Stepanyan, R., Nadariya, M., Hahubia, G., Mahmoud, S., Sakr, K., ArRajehi, A., Paradissis, D., Al-Aydrus, A., Prilepin, M., Guseva, T., Evren, E., Dmitrotsa, A., Filikov, S. V., Gomez, F., Al-Ghazzi, R., Karam, G., 2006. GPS constraints on continental deformation in the Africa-Arabia-Eurasia continental collision zone and implications for the dynamics of plate interactions. J. Geophys. Res. Solid Earth 111, 1–26. https://doi.org/10.1029/2005JB004051

Robinson, A.G., Griffith, E.T., Gardiner, A.R., Home, A.K., 1997. Petroleum geology of the georgian fold and thrust belts and foreland basins, in: Robinson, A.G. (Ed.), Regional and Petroleum Geology of the Black Sea and Surrounding Region: AAPG Memoirs 68. pp. 347–367.

Rolland, Y., 2017. Caucasus collisional history: Review of data from East Anatolia to West Iran. Gondwana Res. 49, 130–146. https://doi.org/10.1016/j.gr.2017.05.005

Rolland, Y., Hässig, M., Bosch, D., Bruguier, O., Melis, R., Galoyan, G., Topuz, G., Sahakyan, L., Avagyan, A., Sosson, M., 2019. The East Anatolia–Lesser Caucasus ophiolite: An exceptional case of large-scale obduction, synthesis of data and numerical modelling. Geosci. Front. 11, 83–108. https://doi.org/10.1016/j.gsf.2018.12.009

Rolland, Y., Perincek, D., Kaymakci, N., Sosson, M., Barrier, E., Avagyan, A., 2012. Evidence for ~80-75Ma subduction jump during Anatolide-Tauride-Armenian block accretion and ~48Ma Arabia-Eurasia collision in Lesser Caucasus-East Anatolia. J. Geodyn. 56–57, 76–85. https://doi.org/10.1016/j.jog.2011.08.006

Rolland, Y., Sosson, M., Adamia, S.A., Sadradze, N., 2011. Prolonged Variscan to Alpine history of an active Eurasian margin (Georgia, Armenia) revealed by 40Ar/39Ar dating. Gondwana Res. 20, 798–815. https://doi.org/10.1016/j.gr.2011.05.007

Sachsenhofer, R.F., 2001. Syn- and post-collisional heat flow in the cenozoic Eastern Alps. Int. J. Earth Sci. 90, 579–592. https://doi.org/10.1007/s005310000179

Sachsenhofer, R.F., Bechtel, A., Gratzer, R., Enukidze, O., Janiashvili, A., Nachtmann, W., Sanishvili, A., Tevzadze, N., Yukler, M.A., 2021. Petroleum Systems in the Rioni and Kura Basins of Georgia. J. Pet. Geol. 44, 287–316. https://doi.org/10.1111/jpg.12794

Sachsenhofer, R.F., Popov, S. V., Coric, S., Mayer, J., Misch, D., Morton, M.T., Pupp, M., Rauball, J., Tari, G., 2018. Paratethyan petroleum source rocks: an overview. J. Pet. Geol. 41, 219–245. https://doi.org/10.1111/jpg.12702

Sangin, S., Buntebarth, G., Weller, A., Melikadze, G., 2018. Temperature Gradient Measurements in Hydrothermal Areas of Georgia. Int. J. Terr. Heat Flow Appl. 1, 14–17. https://doi.org/10.31214/ijthfa.v1i1.7

Schito, A., Andreucci, B., Aldega, L., Corrado, S., Di Paolo, L., Zattin, M., Szaniawski, R., Jankowski, L., Mazzoli, S., 2018. Burial and exhumation of the western border of the Ukrainian Shield (Podolia): a multi-disciplinary approach. Basin Res. 30, 532–549.

https://doi.org/10.1111/bre.12235

Schito, A., Corrado, S., Aldega, L., Grigo, D., 2016. Overcoming pitfalls of vitrinite reflectance measurements in the assessment of thermal maturity: The case history of the lower Congo basin. Mar. Pet. Geol. 74, 59–70. https://doi.org/10.1016/j.marpetgeo.2016.04.002

Sclater, J.G., Christie, P.A.F., 1980. Continental stretching: an explanation of the post-mid-Cretaceous subsidence of the Central North Sea Basin. J. Geophys. Res. 85, 3711–3739.

Shatilova, I.I., Maissuradze, L.S., Koiava, K.P., Kokolashvili, I.M., Bukhsianidze, M.G., Bruch, A.A., 2020. The environmental history of Georgia during the Late Miocene based of foraminifera and pollen. Universal, Tbilisi.

Shaw, J.H., Connors, C., Suppe, J., 2006. Seismic interpretation of contractional fault-related folds. AAPG Studies in Geology, Volume 53. https://doi.org/10.1306/St531003

Sokhadze, G., Floyd, M., Godoladze, T., King, R., Cowgill, E.S., Javakhishvili, Z., Hahubia, G., Reilinger, R., 2018. Active convergence between the Lesser and Greater Caucasus in Georgia: Constraints on the tectonic evolution of the Lesser–Greater Caucasus continental collision. Earth Planet. Sci. Lett. 481, 154–161. https://doi.org/10.1016/j.epsl.2017.10.007

Sosson, M., Rolland, Y., Müller, C., Danelian, T., Melkonyan, R., Kekelia, S., Adamia, S.A., Babazadeh, V., Kangarli, T., Avagyan, A., Galoyan, G., Mosar, J., 2010. Subductions, obduction and collision in the Lesser Caucasus (Armenia, Azerbaijan, Georgia), new insights, in: Sosson, Marc, Kaymakci, N., Stephenson, R.A., Bergerat, F., Starostenko, V. (Eds.), Sedimentary Basin Tectonics from the Black Sea and Caucasus to the Arabian Platform. Geological Society of London, Special Publications 340, pp. 329–352. https://doi.org/10.1144/SP340.14

Sosson, M., Stephenson, R., Sheremet, Y., Rolland, Y., Adamia, S.A., Melkonian, R., Kangarli, T., Yegorova, T., Avagyan, A., Galoyan, G., Danelian, T., Hässig, M., Meijers, M., Müller, C., Sahakyan, L., Sadradze, N., Alania, V., Enukidze, O., Mosar, J., 2016. The eastern Black Sea-Caucasus region during the Cretaceous: New evidence to constrain its tectonic evolution. Comptes Rendus - Geosci. 348, 23–32. https://doi.org/10.1016/j.crte.2015.11.002

Stampfli, G.M., Hochard, C., 2009. Plate tectonics of the Alpine realm, in: Murphy, J.B., Keppie, J.D., Hynes, A.J. (Eds.), Ancient Orogens and Modern Analogues. Geological Society, London, Special Publications 327, pp. 89–111. https://doi.org/10.1144/SP327.6

Stratochem Egypt, 2014. Cuttings & Outcrop Samples_TOC% & Pyrolysis Data.

Sukhishvili, L., Forte, A.M., Merebashvili, G., Leonard, J., Whipple, K.X., Javakhishvili, Z., Heimsath, A., Godoladze, T., 2020. Active deformation and Plio-Pleistocene fluvial reorganization of the western Kura fold-thrust belt, Georgia: Implications for the evolution of the Greater Caucasus Mountains. Geol. Mag. https://doi.org/10.1017/S0016756820000709

Sweeney, J.J., Burnham, A.K., 1990. Evaluation of a Simple Model of Vitrinite Reflectance Based on Chemical Kinetics. Am. Assoc. Pet. Geol. Bull. 74, 1559–1570.

Tari, G., Vakhania, D., Tatishvili, G., Mikeladze, V., Gogritchiani, K., Vacharadze, S., Mayer, J., Sheya, C., Siedl, W., Banon, J.J.M., Sanchez, J.T., 2018. Stratigraphy, structure and petroleum exploration play types of the Rioni Basin, Georgia, in: Simmons, M.D., Tari, G.C., Okay, A.I. (Eds.), Petroleum Geology of the Black Sea. Geological Society, London, Special Publications 464, pp. 403–438. https://doi.org/https://doi.org/10.1144/SP464.14

Tari, G., Vrsic, A., Gumpenberger, T., Mekonnen, E., Hujer, W., Fallah, M., Tevzadze, N., Janiashvili, A., Pace, P., Ricciato, A., Alania, V., Enukidze, O., 2021. Eocene volcaniclastics in the Kartli Basin, Georgia: a fractured reservoir sequence. J. Pet. Geol.

44, 413–433. https://doi.org/10.1111/jpg.12795

Tibaldi, A., Tsereteli, N., Varazanashvili, O., Babayev, G., Barth, A., Mumladze, T., Bonali, F.L., Russo, E., Kadirov, F., Yetirmishli, G., Kazimova, S., 2019. Active stress field and fault kinematics of the Greater Caucasus. J. Asian Earth Sci. 104108. https://doi.org/10.1016/j.jseaes.2019.104108

Tissot, B.P., Welte, D.H., 1978. Petroleum formation and occurrence; a new approach to oil and gas exploration. Springer-Verlag, Berlin, Heidelberg, New York.

Trikhunkov, Y., Kangarli, T.N., Bachmanov, D.M., Frolov, P.D., Shalaeva, E.A., Latyshev, A.V., Simakova, A.N., Popov, S.V., Bylinskaya, M.E., Aliyev, F.A., 2021. Evaluation of Plio-Quaternary uplift of the South-Eastern Caucasus based on the study of the Akchagylian marine deposits and continental molasses. Quat. Int. https://doi.org/10.1016/j.quaint.2021.04.043

Tsereteli, N., Tibaldi, A., Alania, V., Gventsadse, A., Enukidze, O., Varazanashvili, O., Müller, B.I.R., 2016. Active tectonics of central-western Caucasus, Georgia. Tectonophysics 691, 328–344. https://doi.org/10.1016/j.tecto.2016.10.025

USSR Geological Survey, 1971. 1 : 25.000 geological maps of Georgia, Sheet K38.

Vasey, D.A., Cowgill, E., Roeske, S.M., Niemi, N.A., Godoladze, T., Skhirtladze, I., Gogoladze, S., 2020. Evolution of the Greater Caucasus basement and formation of the Main Caucasus Thrust, Georgia. Tectonics 39. https://doi.org/10.1029/2019TC005828

Vermeesch, P., 2009. RadialPlotter: A Java application for fission track, luminescence and other radial plots. Radiat. Meas. 44, 409–410. https://doi.org/10.1016/j.radmeas.2009.05.003

Vincent, S.J., Somin, M.L., Carter, A., Vezzoli, G., Fox, M., Vautravers, B., 2020. Testing models of Cenozoic exhumation in the Western Greater Caucasus. Tectonics 1–27. https://doi.org/10.1029/2018tc005451

Weides, S., Majorowicz, J., 2014. Implications of spatial variability in heat flow for geothermal resource evaluation in large foreland basins: The case of the Western Canada sedimentary basin. Energies 7, 2573–2594. https://doi.org/10.3390/en7042573

Yang, S., Horsfield, B., 2020. Critical review of the uncertainty of Tmax in revealing the thermal maturity of organic matter in sedimentary rocks. Int. J. Coal Geol. 225. https://doi.org/10.1016/j.coal.2020.103500

Yılmaz, A., Adamia, S.A., Chabukiani, A., Chkhotua, T., Erdoğan, K., Tuzcu, S., Karabiyikoğlu, M., 2000. Structural correlation of the southern Transcaucasus (Georgia)-eastern Pontides (Turkey), in: Bozkurt, E., Winchester, J.A., Piper, J.D.A. (Eds.), Tectonics and Magmatism in Turkey and the Surrounding Area. Geological Society of London, Special Publications 173, pp. 171–182.

Yılmaz, A., Adamia, S.A., Yılmaz, H., 2014. Comparisons of the suture zones along a geotraverse from the Scythian Platform to the Arabian Platform. Geosci. Front. 5, 855–875. https://doi.org/10.1016/j.gsf.2013.10.004

Yükler, A., Djavadova, A., Siradze, N., Spiller, R., 2000. The geology, geochemistry and basin modeling of the western Kura Basin depression, Georgia, in: AAPG Regional International Conference. Instanbul, Turkey, July 9-12, 2000.

Figure 1: Main tectonic units and structures of the Eastern Anatolia-Caucasus region superimposed on an ASTER GDEM shaded relief map (source: USGS) (modified after Gusmeo et al., 2021; tectonic structures after Cavazza et al., 2019; Forte et al., 2014; Sosson et al., 2010). ASASZ = Amasia-Sevan-Akera suture zone; D = Dzirula Massif; IAESZ = Izmir-Ankara-Erzinçan suture zone; K = Khrami Massif; L = Loki Massif; MCT = Main Caucasian Thrust. Red lines with triangles indicate thrusts; red lines are normal, strike-slip or unknown kinematics faults. Dashed rectangle indicates location of Figures 2 and 12. Inset: Tectonic sketch map of the Arabia-Eurasia collision zone, after Cavazza et al. (2019) and Sosson et al. (2010). Red arrows represent selected GPS vectors after Reilinger et al. (2006); numbers indicate relative displacement with respect to stable Eurasia (in mm/yr). EAF = East Anatolian Fault; NAF = North Anatolian Fault.

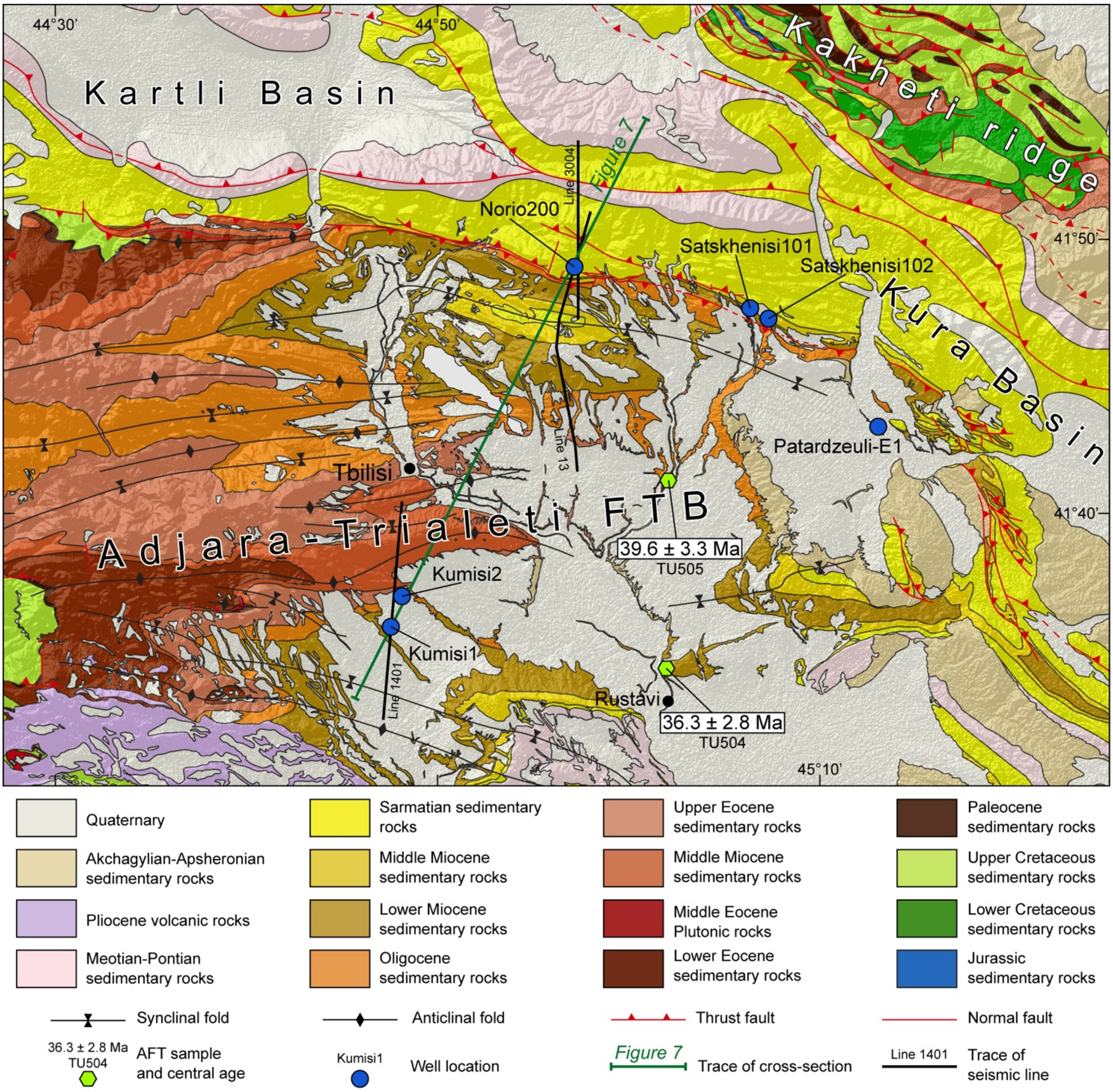

Figure 2: Geological map of the study area (USSR Geological Survey, 1971), with location of the six wells considered in this study, the two samples analysed for AFT inverse modelling, and the three seismic reflection profiles interpreted to build the cross-section in Figure 7. The trace of the cross-section in Figure 7 is also shown. Map location is indicated in Figure 1. See Figure 3 for regional stratigraphic stages.

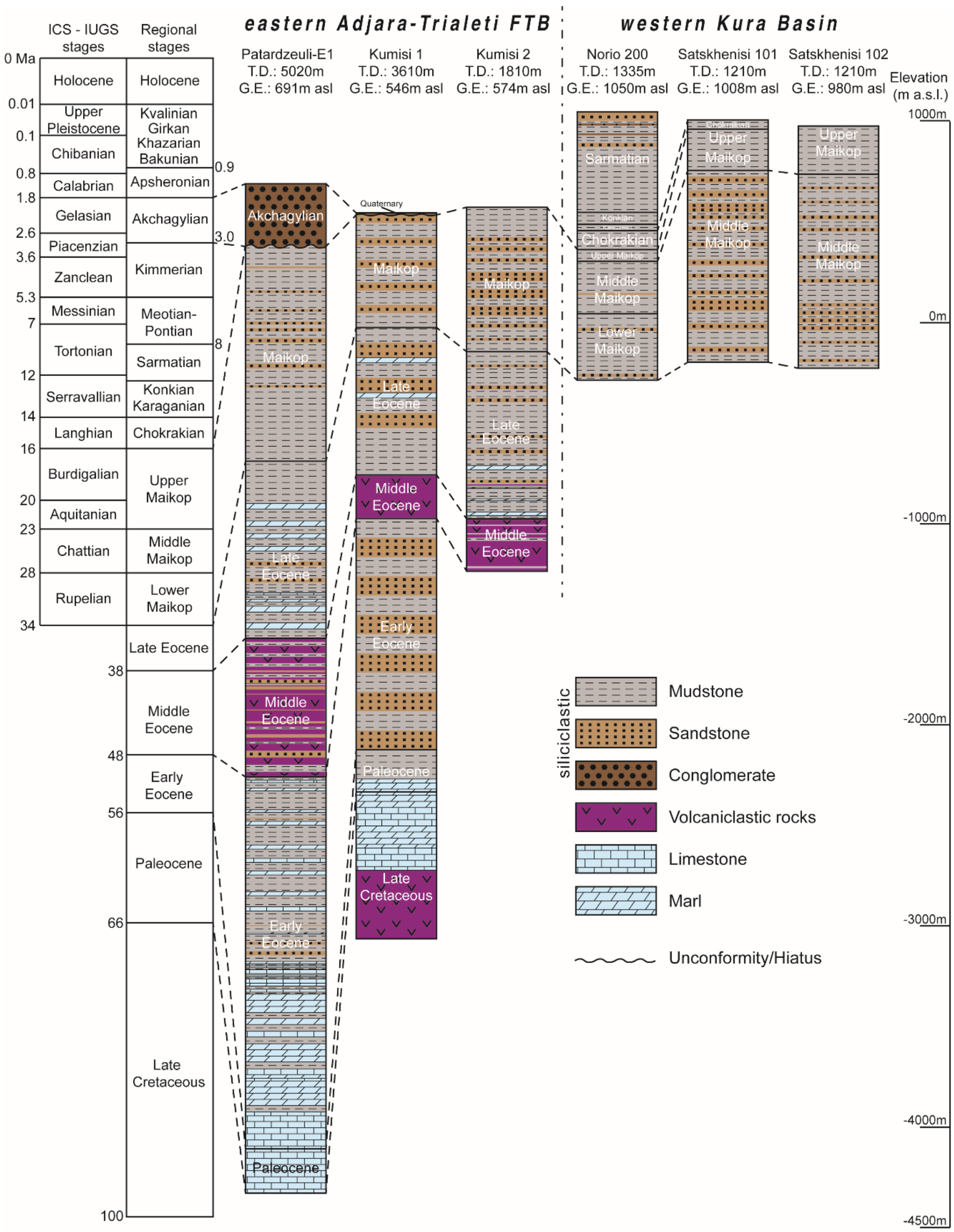

Figure 3: Detailed stratigraphy of the six wells analysed in this study, with total depth (T.D.) and ground elevation (G.E.) of the opening pit reported for each well. The chronostratigraphic chart at the left side is after Adamia et al. (2010), Lazarev et al. (2019) and Neubauer et al. (2015). Numerical ages after Cohen et al. (2021).

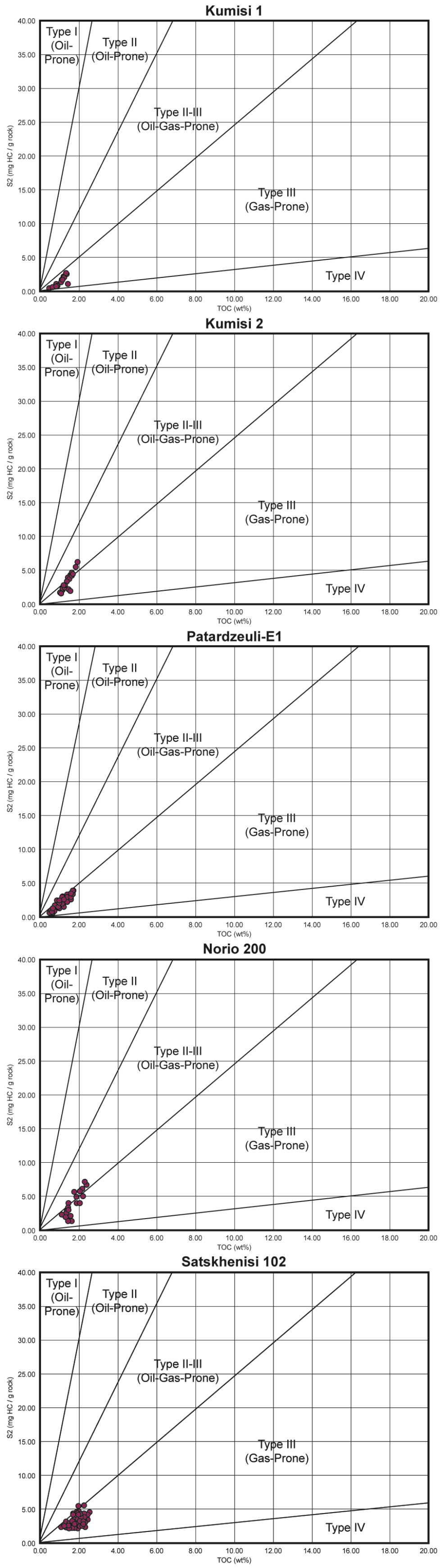

Figure 4: TOC vs S2 plots for the five wells for which thermal maturity data are available, showing the kerogen type of each data (prevailing Type III, alternatively Type II-III). Data from DIG (2014), Sachsenhofer et al. (2021), Stratochem Egypt (2014). See Supplementary Materials Figs. S1, S2, S3, S4, S5 for additional diagrams showing kerogen types with greater detail.

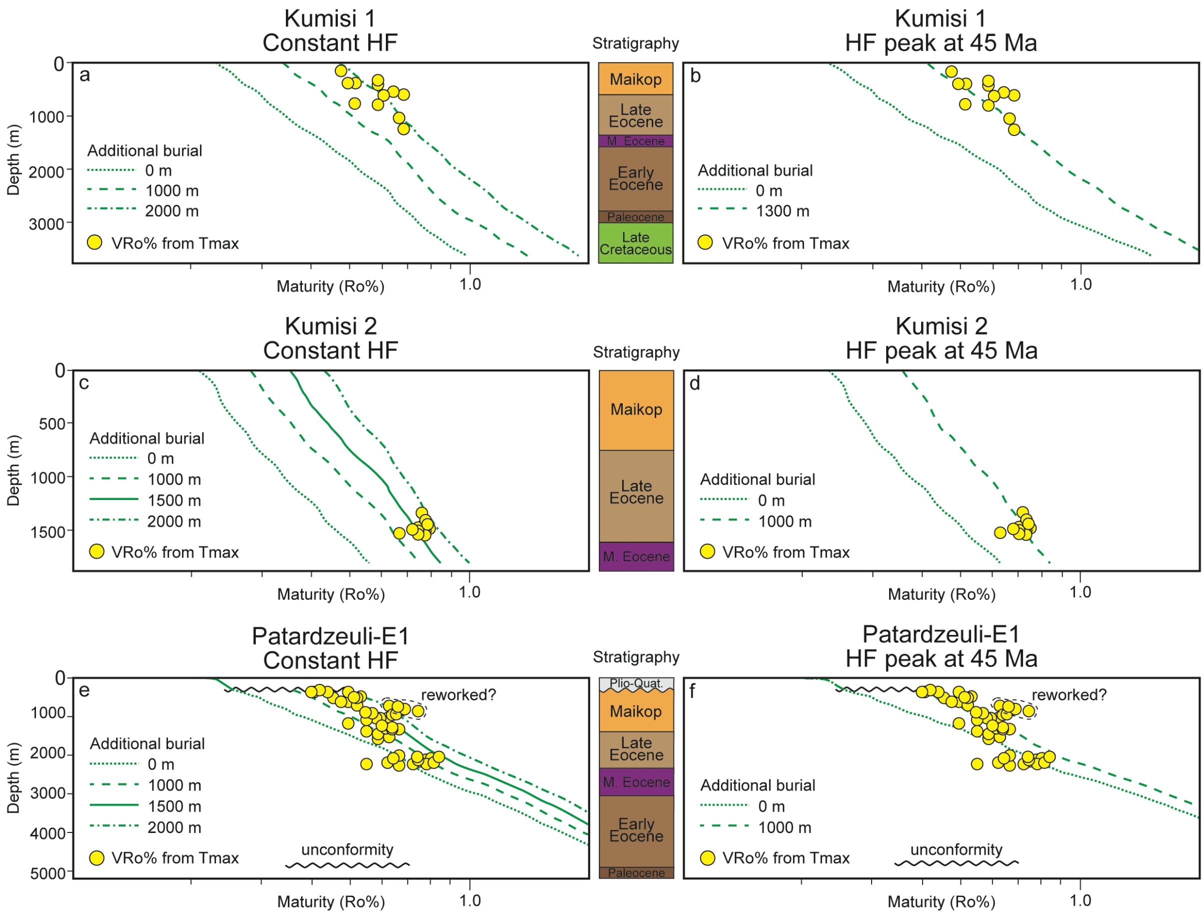

Figure 5: Sensitivity analysis for the three wells located in eastern Adjara-Trialeti FTB (see Fig. 2 for location), showing the different fitting of thermal maturity data with various amounts of additional burial, assuming a constant heat flow (a, c, and e) or a rifting model with an HF peak around 45 Ma (b, d and f). Data from Sachsenhofer et al. (2021), Stratochem Egypt (2014).

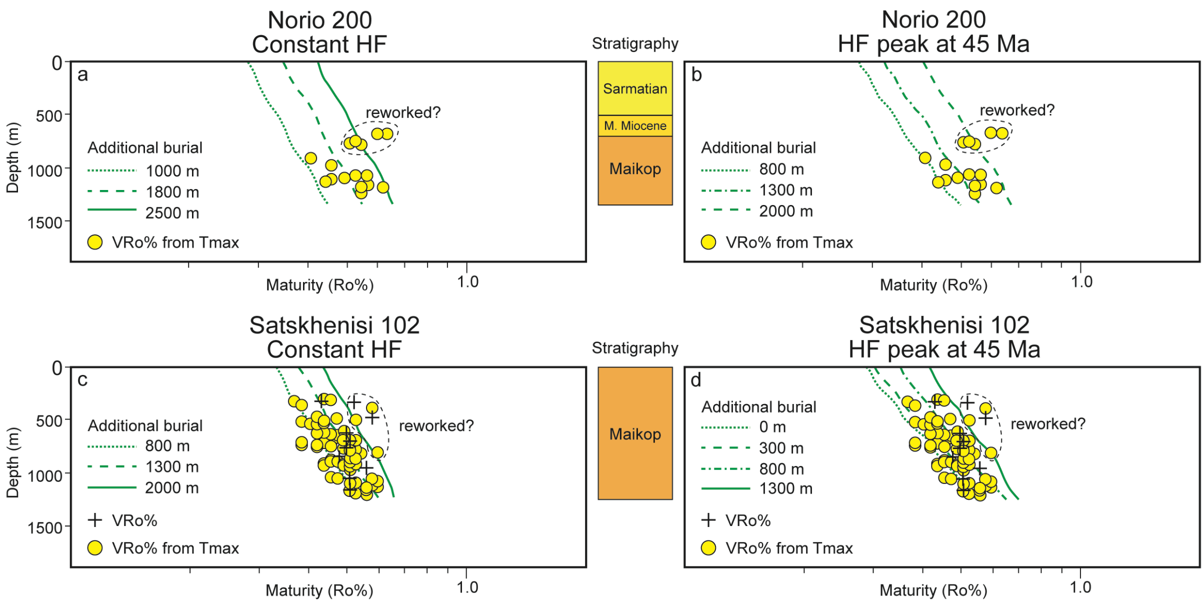

Figure 6: Sensitivity analysis for two of the wells located in the western Kura Basin (see Fig. 2 for location), showing the different fitting of thermal maturity data with various amounts of additional burial, assuming a constant heat flow (a, c) or a rifting model with an HF peak around 45 Ma (b and d). Data from DIG (2014), Sachsenhofer et al. (2021).

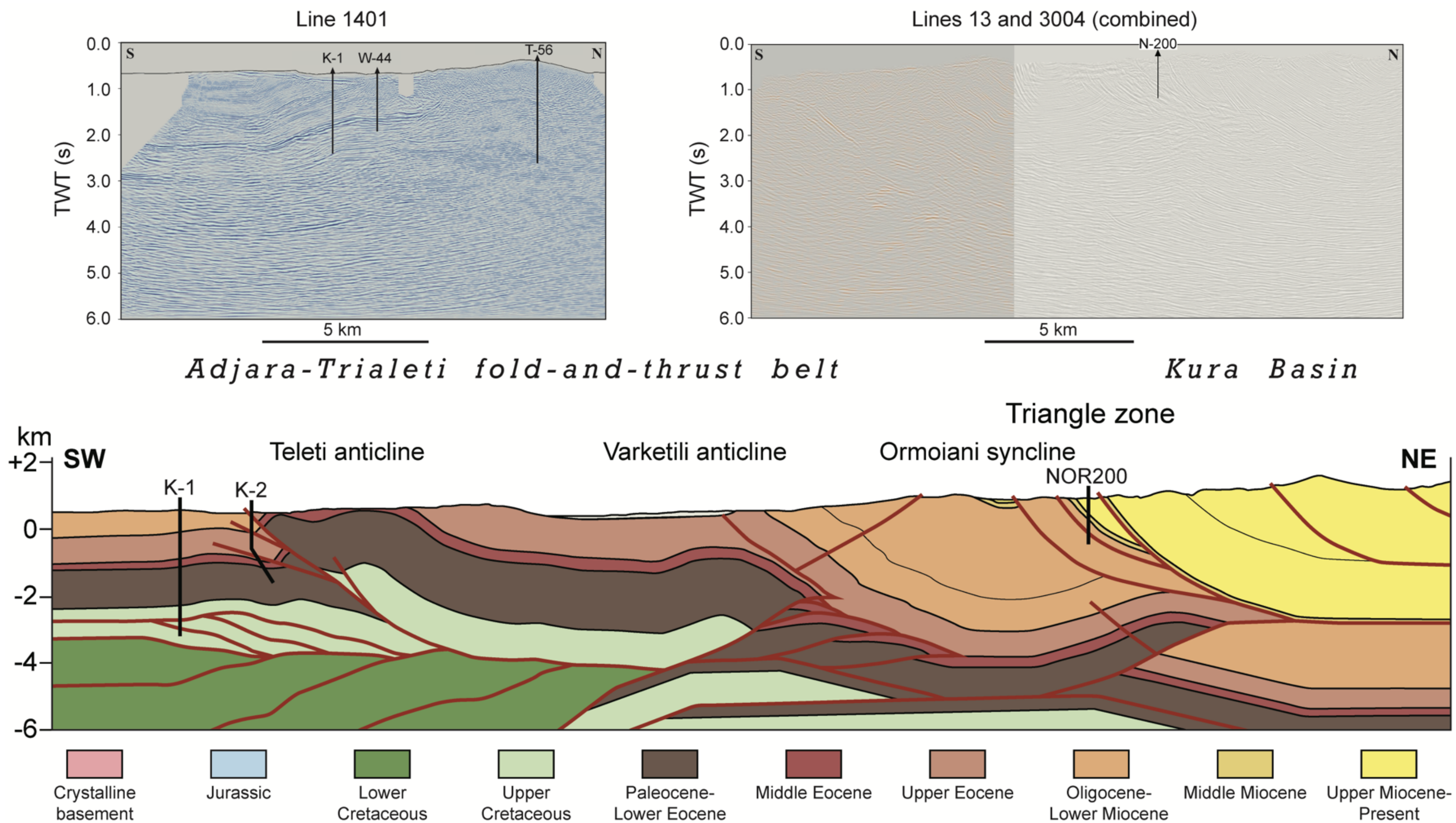

Figure 7: Geological cross-section based on the interpretation of three depth-migrated seismic reflection profiles (lines 1401, 13 and 3004) across the eastern Adjara-Trialeti FTB and the western Kura Basin. Uninterpreted seismic profiles are reported on top. Seismic interpretation by V. Alania and P. Pace integrates also surface data, from geological maps (USSR Geological Survey, 1971) and field observations, and wells data. Wells are

projected on the section (K-1 = Kumisi 1; K-2 = Kumisi 2; NOR200 = Norio 200). Original seismic data courtesy of Georgia Oil & Gas Limited.

No vertical exaggeration. See Figure 2 for location of cross-section and seismic profiles.

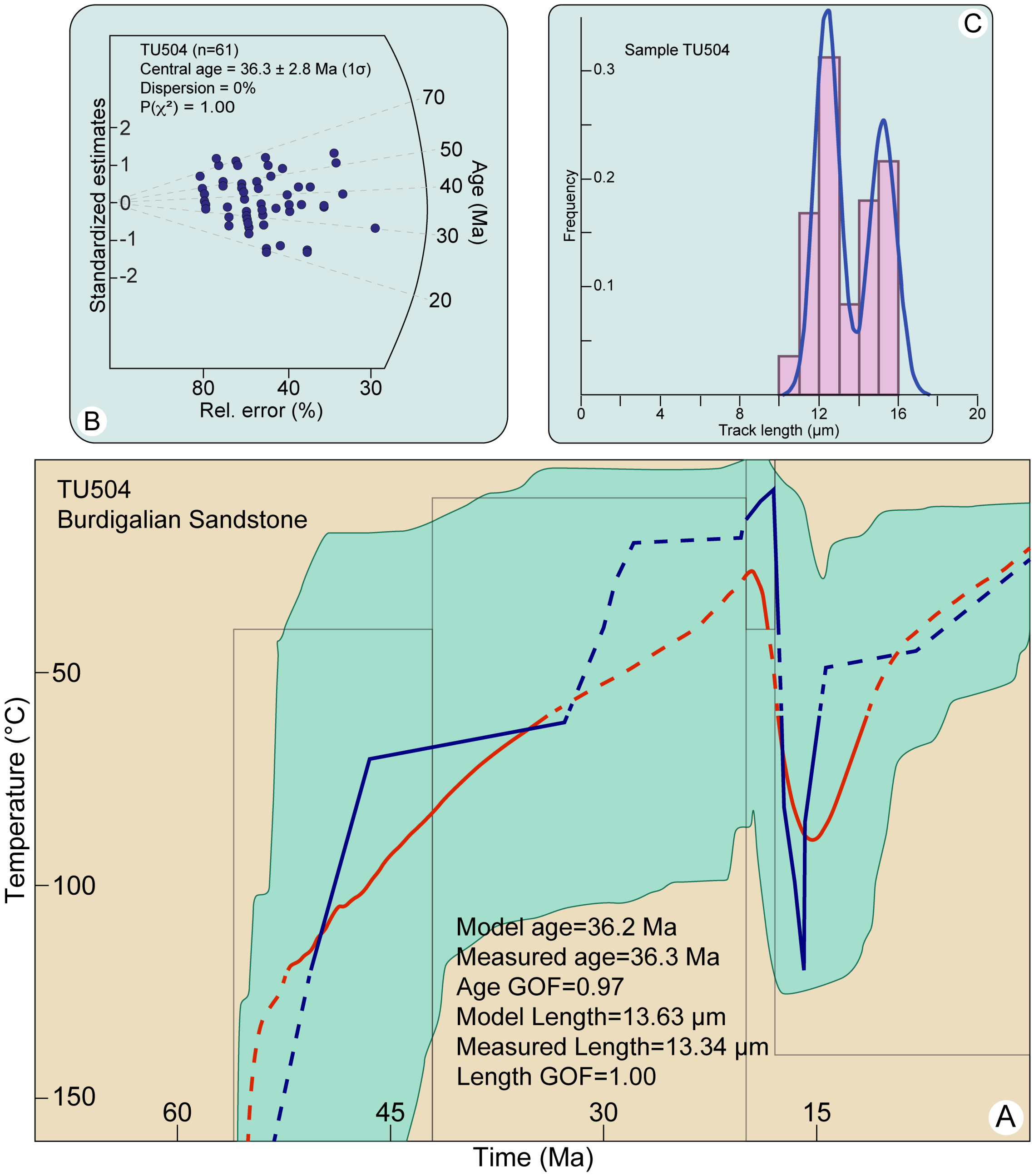

Figure 8: A) Time-temperature path obtained from inverse modelling of sample TU504. See Fig. 2 for sample location. Green area marks the envelope of all thermal histories that have a good (>0.5) fit with the data, red line represents the mean of all good paths, and the blue line is the best-fit time-temperature path. Parameters related to inverse modelling are reported: GOF, goodness-of-fit, gives an indication about the fit between observed and predicted data (values closer to 1 are best). B) Radial plot of single-grain AFT ages. C) D) Confined-track length frequency distribution.

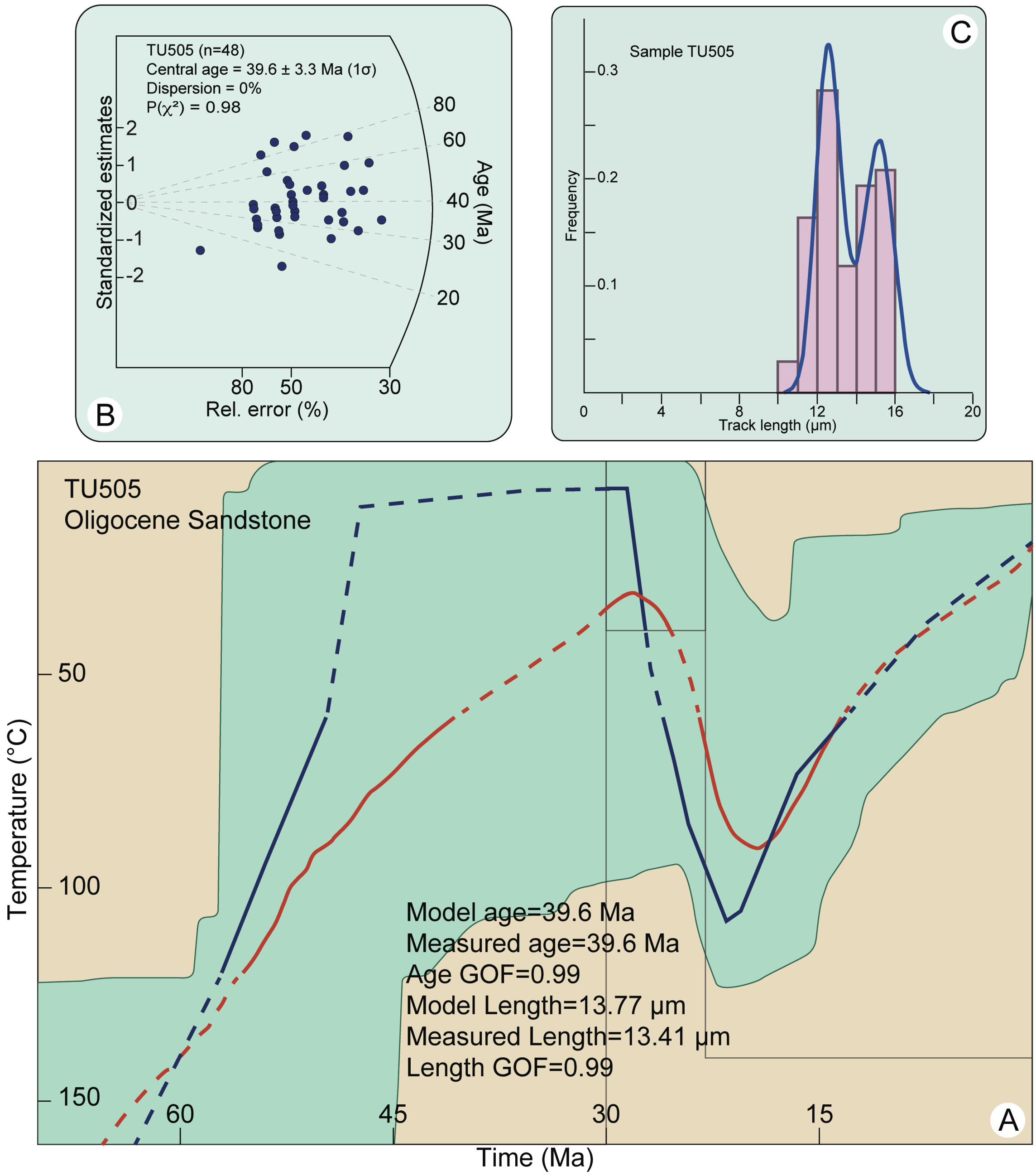

Figure 9: A) Time-temperature path obtained from inverse modelling of sample TU505. See Fig. 2 for sample location. Green area marks the envelope of all thermal histories that have a good (>0.5) fit with the data, red line represents the mean of all good paths, and the blue line is the best-fit time-temperature path. Parameters related to inverse modelling are reported: GOF, goodness-of-fit, gives an indication about the fit between observed and predicted data (values closer to 1 are best). B) Radial plot of single-grain AFT ages. C) Confined-track length frequency distribution.

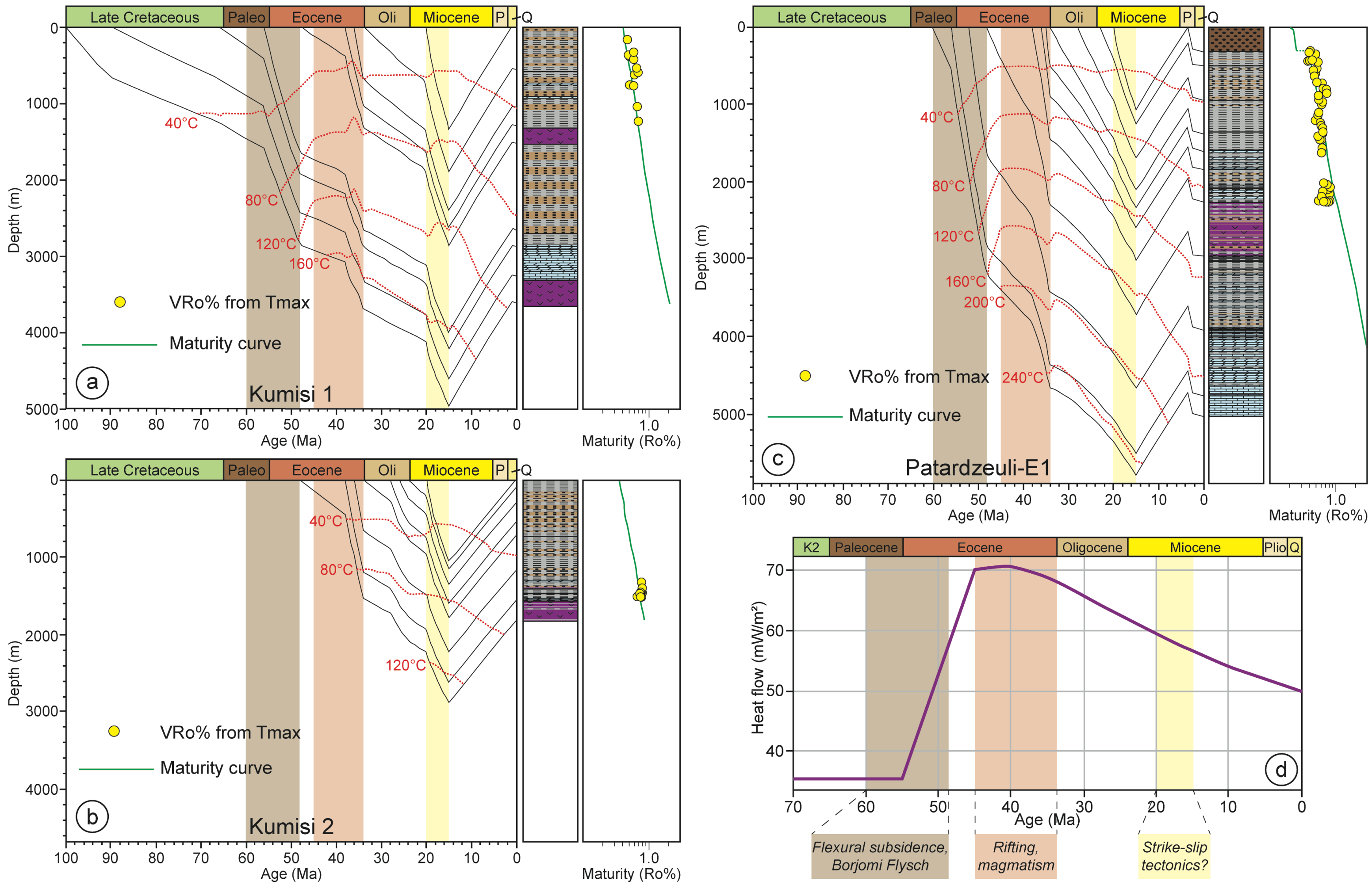

Figure 10: 1D burial and thermal history for the Kumisi 1 (a), Kumisi 2 (b) and Patardzeuli-E1 (c) wells, located in the eastern Adjara-Trialeti fold-and-thrust belt. See Fig. 2 for location. The models are calibrated against Tmax data. A rifting heat-flow model, with a peak around 45 Ma, was used for modelling (d). Vertical bars highlight the main subsidence pulses and the related tectonic events (see text for further discussion).

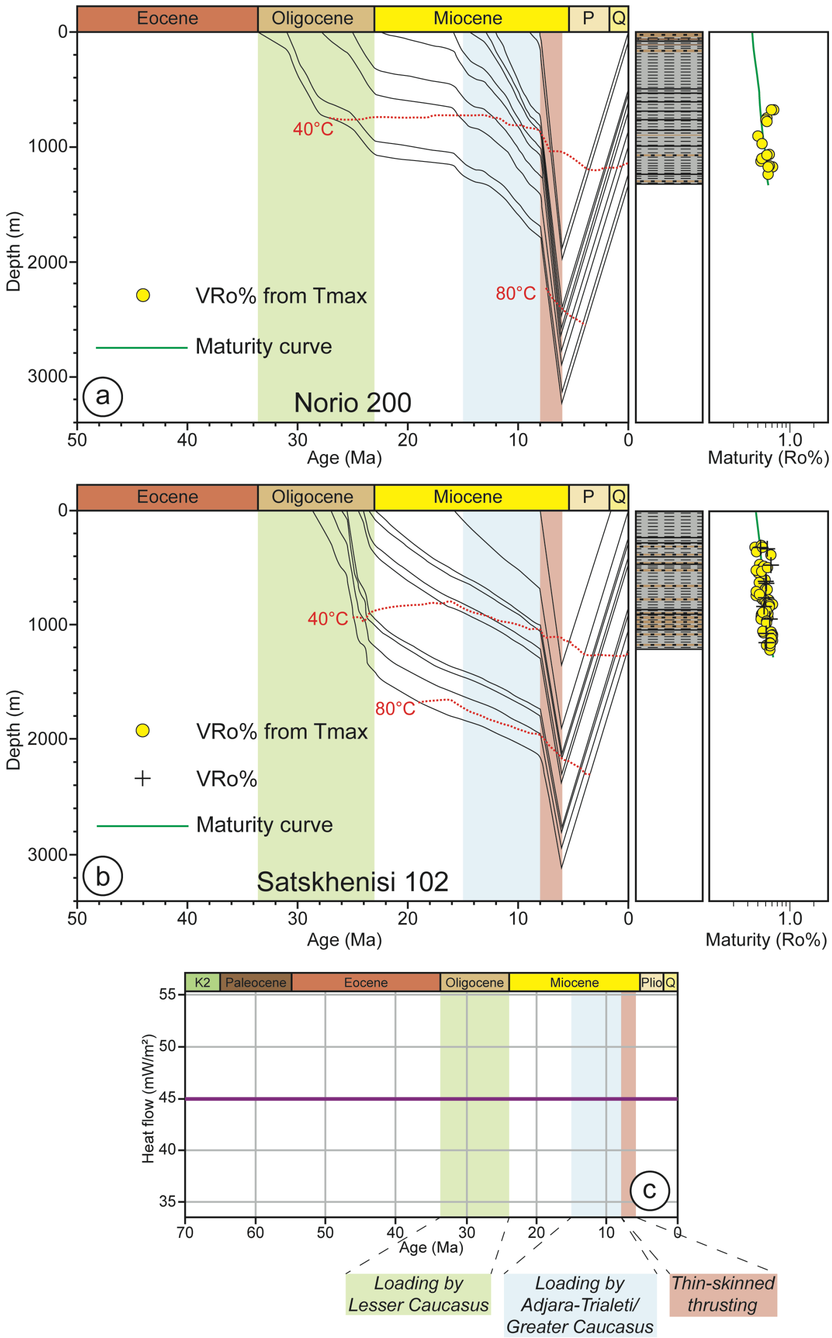

Figure 11: 1D burial and thermal history for the Norio 200 (a) and Satskhenisi 102 (b) wells, located in the western Kura Basin. See Fig. 2 for location. The models are calibrated against Tmax data (Norio 200) and Tmax and vitrinite reflectance data (Satskhenisi 102). A steady-state heat flow of 45 mW/m^2 was adopted (c). Vertical bars highlight the main subsidence pulses and the related tectonic events (see text for further discussion).

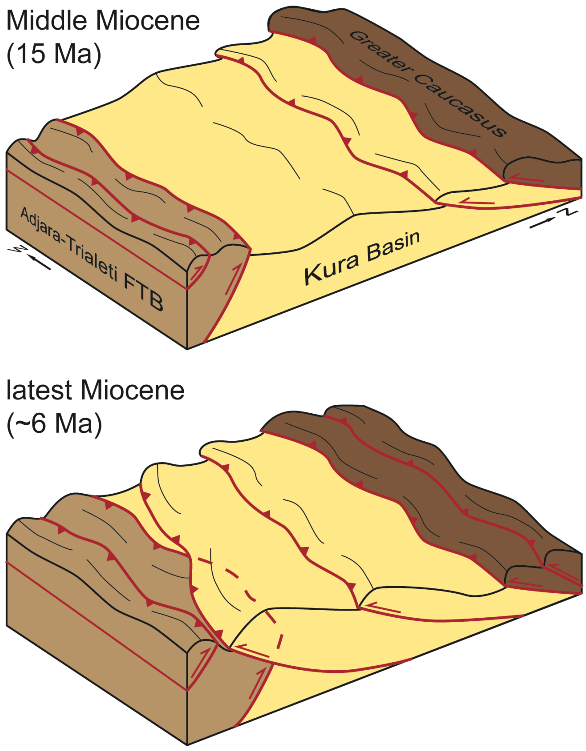

Figure 12: Block diagrams showing the Cenozoic tectonic evolution of the eastern Adjara-Trialeti FTB-western Kura Basin system (see Fig. 1 for location) as reconstructed in this paper. During the Middle Miocene the Kura Basin experienced cumulative subsidence due to structural inversion of the Adjara-Trialeti basin and southward propagation of the Greater Caucasus deformation front. In the latest Miocene south-directed thrusts reached the southern margin of the Kura Basin and covered the eastern Adjara-Trialeti FTB, forcing its eastward plunge. To the west the south-directed thrusts affecting the Kura Basin and the north-directed structures of the Adjara-Trialeti FTB were not yet interfering.

Table 1: Results of apatite fission-track analyses (see Fig. 2 for location of samples).

Sample	Rock Type	Age	Location	Elevation (m)	UTM Coordinates	No. crystals	Spontaneous		Induced		$P(\chi^2)$	Dosimeter		Age (Ma) ± 1s	MCTL (µm) ± standard error	Standard deviation	No. tracks measured	Mean D-par
							ρ_s	N_s	ρ_i	N_i		ρ_d	N_d					
TU504	Sandstone	Early Miocene (Burdigalian)	Eastern ATFTB	396	38T 0500933 4602375	61	0.15	333	0.81	1770	99.98	11.64	7276	36.3 ± 2.8	13.34 ± 0.17	1.57	83	2.75
TU505	Sandstone	middle-late Oligocene	Eastern ATFTB	512	38T 0500906 4615010	48	0.24	270	1.17	1307	97.99	11.57	7230	39.6 ± 3.3	13.41 ± 0.18	1.47	67	2.31

ATFTB = Adjara-Trialeti fold-and-thrust belt. MCTL = mean confined tracks length. Central ages are calculated using dosimeter U-free mica CN5 as external detector and $\zeta = 332.68 \pm 16.54$ (analyst T. Gusmeo); ρ_s= spontaneous track densities (x 10^5 cm^{-2}) measured in internal mineral surfaces; Ns= total number of spontaneous tracks; ρ_i and ρ_d= induced and dosimeter track densities (x 10^6 cm^{-2}) on external mica detectors (g= 0.5); N_i and N_d= total number of induced and dosimeter tracks; $P(\chi^2)$= probability of obtaining χ^2-value for n degrees of freedom (n= number of crystals-1): a probability >5% is indicative of a homogeneous population.

Table 2: Summary of thermal maturity data used as input for wells modelling. Average, minimum and maximum values of TOC (>0.5%), Rock-Eval Pyrolysis data (S1, S2, S3, Tmax, HI, OI) and vitrinite reflectance data (either measured in situ or calculated from Tmax) are provided, subdivided for age interval in each well analysed. Equivalent VR$_o$% in the Satskhenisi 102 well was calculated from Tmax using the equation by Jarvie et al. (2001). Data derive from DIG (2014), Sachsenhofer et al. (2021) and Stratochem Egypt (2014), and were kindly provided by the GOGC.

Well name	**GPS Coordinates (UTM Zone 38N)**	**Samples depth interval (m)**	**Age of interval**	**N° samples**	**TOC (>0.5) (%) Average min, max**	**S1 (mg/g) Average min, max**	**S2 (mg/g) Average min, max**	**S3 (mg/g) Average min, max**	**Tmax (°C) Average min, max**	**HI (mgHC/gTOC) Average min, max**	**OI (mgCO2/gTOC) Average min, max**	**VR$_o$% (measured) Average min, max**	**VR$_o$% (calculated from Tmax) Average min, max**
Kumisi 1	0482387 4605231	165-425	Maikop (Oligocene)	5	1.09 0.82, 1.46	0.08 0.05, 0.11	1.17 0.74, 1.72	1.17 0.75, 1.52	429 426, 432	107 73, 146	117 51, 185	- -	- -
		555-1245	Late Eocene	9	1.01 0.52, 1.36	0.08 0.05, 0.10	1.47 0.38, 2.67	0.92 0.66, 1.34	434 428, 437	136 74, 196	102 53,196	- -	- -
Kumisi 2	0483141 4607313	1340-1535	Late Eocene	21	1.44 1.05, 1.95	0.16 0.05, 0.27	3.30 1.55, 6.20	- -	439 434, 441	222 117, 318	- -	- -	- -
Patardzeuli	0515117 4618697	330-1350	Maikop (Oligocene-Early Miocene)	35	1.01 0.64, 1.26	0.15 0.08, 0.27	1.63 0.64, 2.92	- -	430 422, 440	158 96, 238	- -	- -	- -
		1380-2260	Late Eocene	45	1.18 0.59, 1.77	0.24 0.06, 0.55	1.98 0.57, 3.75	- -	436 430, 445	160 97, 212	- -	- -	- -
Norio 200	0494735 4629461	665-675	Chokrakian	2	1.42 1.37, 1.46	0.16 0.14, 0.18	3.38 2.71, 4.04	- -	431 430, 432	238 198, 277	- -	- -	- -
		745-966	Middle Maikop (Late Oligocene)	5	1.47 1.13, 2.51	0.20 0.12, 0.24	2.83 1.36, 4.09	- -	424 419, 427	191 93, 228	- -	- -	- -
		1062-1233	Lower Maikop (Early Oligocene)	12	1.96 1.32, 2.93	0.28 0.06, 0.46	4.75 1.48, 7.13	- -	426 421, 431	234 90, 318	- -	- -	- -
Satskhenisi 101	0506512 4626657	-	-	-	-	-	-	-	-	-	-	-	-
Satskhenisi 102	0507754 4625925	309-1205	Middle Maikop (Late Oligocene)	78	1.88 0.50, 2.58	- -	2.85 2.05, 5.43	- -	424 417, 430	175 90, 260	55 25, 85	0.51 0.43, 0.56	0.48 0.35, 0.58

Table 3: Lithological data used as input for wells modelling, subdivided for each well. Keys for abbreviations are: mds = mudstone; sds = sandstone; cng = conglomerate; lms = limestone; tff = tuff.

Kumisi 1

Event name	Type	End Age (Ma)	Top depth (m)	Present thickness (m)	Eroded thickness (m)	Lithology				
						mds (%)	sds (%)	cng (%)	lms (%)	tff (%)
Quaternary	Formation	0.1	0	10	-	-	-	100	-	-
Erosion	Erosion	1	-	-	-1.300	-	-	-	-	-
Deposition (Maikop)	Deposit	15	-	-	1.300	100	-	-	-	-
Maikop	Formation	20	10	560	-	70	30	-	-	-
Late Eocene	Formation	34	570	500	-	45	45	-	10	-
	Formation	36	1.070	233	-	100	-	-	-	-
Middle Eocene	Formation	38	1.303	217	-	-	-	-	-	100
Early Eocene	Formation	48	1.520	1.150	-	50	50	-	-	-
Paleocene	Formation	56	2.670	210	-	70	-	-	30	-
Late Cretaceous	Formation	66	2.880	390	-	-	-	-	100	-
	Formation	90	3.270	339	-	-	-	-	-	100

Kumisi 2

Event name	Type	End Age (Ma)	Top depth (m)	Present thickness (m)	Eroded thickness (m)	Lithology				
						mds (%)	sds (%)	cng (%)	lms (%)	tff (%)
Erosion	Erosion	1	-	-	-1.000	-	-	-	-	-
Deposition (Maikop)	Deposit	15	-	-	1.000	100	-	-	-	-
Maikop	Formation	20	0	100	-	100	-	-	-	-
	Formation	24	100	190	-	60	40	-	-	-
	Formation	26	290	250	-	40	60	-	-	-
	Formation	28	540	180	-	90	10	-	-	-
Late Eocene	Formation	34	720	440	-	90	10	-	-	-
	Formation	36	1.160	390	-	80	10	-	10	-
Middle Eocene	Formation	38	1.550	260	-	-	-	-	-	100

Patardzeuli-E1

Event name	Type	End Age (Ma)	Top depth (m)	Present thickness (m)	Eroded thickness (m)	Lithology				
						mds (%)	sds (%)	cng (%)	lms (%)	tff (%)
Quaternary	Formation	0.1	0	40	-	-	-	100	-	-
Akchagylian	Formation	2.5	40	270	-	-	-	100	-	-
Erosion	Erosion	3.5	-	-	-1.000	-	-	-	-	-
Deposition (Maikop)	Deposit	15	-	-	1.000	100	-	-	-	-
Maikop	Formation	20	310	195	-	100	-	-	-	-
	Formation	23	505	445	-	80	20	-	-	-
	Formation	28	950	415	-	90	10	-	-	-
Late Eocene	Formation	34	1.365	225	-	100	-	-	-	-
	Formation	35	1.590	260	-	60	-	-	40	-
	Formation	36	1.850	410	-	80	20	-	-	-
Middle Eocene	Formation	38	2.260	690	-	-	-	-	-	100
Early Eocene	Formation	48	2.950	960	-	70	-	-	30	-
	Formation	52	3.910	840	-	20	-	-	80	-
Paleocene	Formation	56	4.750	270	-	-	-	-	100	-

Norio 200

Event name	Type	End Age (Ma)	Top depth (m)	Present thickness (m)	Eroded thickness (m)	Lithology				
						mds (%)	sds (%)	cng (%)	lms (%)	tff (%)
Erosion	Erosion	0.1	-	-	-1.800	50	50	-	-	-
Deposition (Late Miocene)	Deposit	6	-	-	1.800	50	50	-	-	-
Sarmatian	Formation	8	0	85	-	50	50	-	-	-
	Formation	9	85	415	-	80	20	-	-	-
Konkian	Formation	12	500	60	-	100	-	-	-	-
Karaganian	Formation	13	560	30	-	100	-	-	-	-
Chokrakian	Formation	14.5	590	95	-	100	-	-	-	-
Upper Maikop (Early Miocene)	Formation	16	685	55	-	100	-	-	-	-
Middle Maikop (Late Oligocene)	Formation	23	740	130	-	100	-	-	-	-
	Formation	25	870	132	-	90	10	-	-	-
Lower Maikop (Early Oligocene)	Formation	28	1.002	250	-	100	-	-	-	-
	Formation	31	1.252	83	-	90	10	-	-	-

Satskhenisi 102

Event name	Type	End Age (Ma)	Top depth (m)	Present thickness (m)	Eroded thickness (m)	Lithology				
						mds (%)	sds (%)	cng (%)	lms (%)	tff (%)
Erosion	Erosion	0.1	-	-	-1.800	50	50	-	-	-
Deposition (Middle-Late Miocene)	Deposit	6	-	-	1.300	50	50	-	-	-
Deposition (Middle-Late Miocene)	Deposit	8	-	-	500	50	50	-	-	-
Upper Maikop (Early Miocene)	Formation	16	0	240	-	100	-	-	-	-
Middle Maikop (Late Oligocene)	Formation	23	240	30	-	100	-	-	-	-
	Formation	23.5	270	135	-	90	10	-	-	-
	Formation	24	405	60	-	60	40	-	-	-
	Formation	24.5	465	390	-	80	20	-	-	-
	Formation	25.5	855	45	-	60	40	-	-	-
	Formation	26	900	140	-	50	50	-	-	-
	Formation	27	1040	170	-	90	10	-	-	-